MONTANA
Department of Transportation
Research

# CONCRETE-FILLED STEEL TUBE TO CONCRETE PILE CAP CONNECTIONS – FURTHER EVALUATION/IMPROVEMENT OF ANALYSIS/DESIGN METHODOLOGIES

*FHWA/MT-24-003/9630-628*

## Final Report

March 2024

*prepared for*

THE STATE OF MONTANA DEPARTMENT OF TRANSPORTATION

*in cooperation with*

THE U.S. DEPARTMENT OF TRANSPORTATION
FEDERAL HIGHWAY ADMINISTRATION

March 2024

*prepared by*

Michael Berry, PhD
Cash Cota
Kirsten Matteson, PhD

Montana State University
Bozeman, MT

# CONCRETE-FILLED STEEL TUBE TO CONCRETE PILE CAP CONNECTIONS – FURTHER EVALUATION/IMPROVEMENT OF ANALYSIS/DESIGN METHODOLOGIES

*Final Report*

Prepared by:

Michael Berry, PhD
Professor

Cash Cota
Graduate Research Assistant

Kirsten Matteson, PhD
Assistant Professor

of the

**Civil Engineering Department**
**Western Transportation Institute**
Norm Asbjornson College of Engineering
Montana State University – Bozeman

Prepared for:

**Montana Department of Transportation**
Research Programs
2701 Prospect Avenue
P.O. Box 201001
Helena, Montana 59620-1001

March 2024

# TECHNICAL REPORT DOCUMENTATION PAGE

| | | | |
|---|---|---|---|
| 1. Report No.<br>FHWA/MT-24-003/9630-628 | 2. Government Access No. | 3. Recipient's Catalog No. | |
| 4. Title and Subtitle<br>Concrete-Filled Steel Tube to Concrete Pile Cap Connections – Further Evaluation/Improvement of Analysis/Design Methodologies | | 5. Report Date<br>March 2024<br>6. Performing Organization Code | |
| 7. Author(s)<br>Michael Berry (0000-0003-2134-9335), Cash Cota (0009-0001-2521-4369), and Kirsten Matteson (0000-0001-9367-6867) | | 8. Performing Organization Report Code | |
| 9. Performing Organization Name and Address<br>Civil Engineering<br>Western Transportation Institute<br>PO Box 174250<br>Montana State University – Bozeman<br>Bozeman, Montana 59717-4250 | | 10. Work Unit No. (TRAIS)<br>11. Contract or Grant No.<br>MSU G&C # 4W9975<br>MDT Project #9630-628 | |
| 12. Sponsoring Agency Names and Addresses<br>Research Programs<br>Montana Department of Transportation (SPR)<br>http://dx.doi.org/10.13039/100009209<br>2701 Prospect Avenue<br>PO Box 201001<br>Helena MT 59620-1001 | | 13. Type of Report and Period Covered<br>Final Report<br>July 2018 – March 2024<br>14. Sponsoring Agency Code<br>5401 | |
| 15. Supplementary Notes<br>This report can be found at https://www.mdt.mt.gov/research/projects/structures/seismic.aspx DOI: https://doi.org/10.21949/1529560.<br><br>Recommended Citation:<br>Berry, M., Cota, C., Matteson, K. (2024). Concrete-Filled Steel Tube to Concrete Pile Cap Connections – Further Evaluation/Improvement of Analysis/Design Methodologies (FHWA/MT-24-003/9630-628). Helena, MT: Montana Department of Transportation. https://doi.org/10.21949/1529560. | | | |
| 16. Abstract<br>This research project focuses on the structural behavior of concrete-filled steel tube (CFST) to concrete pile cap connections, a critical component in many Montana bridges. A series of four experimental pile cap connection specimens were designed and tested to assess the influence of key parameters such as specimen scale, concrete strength, and the incorporation of U-bars on the overall connection performance. The findings from this research revealed that all specimens, barring the specimen with U-bars, displayed consistent moment-drift responses, damage progression, and failure mechanisms within the concrete cap. The inclusion of U-bars notably increased the connection capacity by about 50%, altering the failure mechanism to a plastic hinge formation in the CFST pile. Additionally, the study validated the efficacy of a novel moment-rotation methodology for predicting the capacity of cap connections, with an average measured-to-predicted ratio of 0.95 and a coefficient of variation of 10%. However, this methodology showed a tendency to overpredict capacities in connections without U-bars and underpredict in those with U-bars. Overall, this research provides valuable insight into the behavior of these critical connections under diverse conditions and demonstrates the efficacy of the moment-rotation methodology. | | | |
| 17. Key Words<br>Bridge piers, Concrete structures, Design methods, Load tests, Piles (Supports), Reinforcement (Engineering) | | 18. Distribution Statement<br>No restrictions. This document is available through NTIS, Springfield, Virginia 22161. | |
| 19. Security Classif. (of this report)<br>Unclassified | 20. Security Classif. (of this page)<br>Unclassified | 21. No. of Pages<br>66 | 22. Price |

# DISCLAIMER STATEMENT

This document is disseminated under the sponsorship of the Montana Department of Transportation (MDT) and the United States Department of Transportation (USDOT) in the interest of information exchange. The State of Montana and the United States assume no liability for the use or misuse of its contents.

The contents of this document reflect the views of the authors, who are solely responsible for the facts and accuracy of the data presented herein. The contents do not necessarily reflect the views or official policies of MDT or the USDOT.

The State of Montana and the United States do not endorse products of manufacturers.

This document does not constitute a standard, specification, policy or regulation.

# ALTERNATIVE FORMAT STATEMENT

Alternative accessible formats of this document will be provided on request. Persons who need an alternative format should contact the Office of Civil Rights, Department of Transportation, 2701 Prospect Avenue, PO Box 201001, Helena, MT 59620. Telephone 406-444-5416 or Montana Relay Service at 711.

# ACKNOWLEDGMENTS

The authors would like to acknowledge the financial support for this project provided by the Montana Department of Transportation (MDT). The authors would also like to recognize and thank the MDT Research Section and the technical panel for their participation in this project, particularly Lenci Kappes. Furthermore, the authors would like to acknowledge Concrete Connections out of Bozeman, Montana for their efforts in bending the rebar used in this research. Their workmanship, timeliness, and generosity were vital to the success of the project. Additionally, this research would not have been possible without the support of several undergraduate and graduate student research assistants. In particular, the authors would like to thank James Starke, Emtiaz Ahmed, Jake Artis, Dawson Peterman, Axel Tanner, and Ethan Turner for their diligent help in the lab during both construction and testing phases of the project. The authors would also like to thank Instructor Tim White for his help throughout the entire duration of the project on various technical components where experience and good judgement was necessary.

# UNIT CONVERSIONS

| Measurement | Metric | English |
|---|---|---|
| Length | 1 cm | 0.394 in |
| | 1 m | 3.281 ft |
| | 1 km | 0.621 mile |
| Area | 1 $cm^2$ | 0.155 $in^2$ |
| | 1 $m^2$ | 1.196 $yd^2$ |
| Volume | 1 $m^3$ | 1.308 $yd^3$ |
| | 1 ml | 0.034 oz |
| Force | 1 N | 0.225 lbf |
| | 1 kN | 0.225 kip |
| Stress | 1 MPa | 145 psi |
| | 1 GPa | 145 ksi |
| Unit Weight | 1 $kg/m^3$ | 1.685 $lbs/yd^3$ |
| Velocity | 1 kph | 0.621 mph |

# TABLE OF CONTENTS

# LIST OF FIGURES

# LIST OF TABLES

# 1 INTRODUCTION

## 1.1 Background

The Montana Department of Transportation (MDT) has found concrete-filled steel tube (CFST) piles connected at the top by a concrete pile cap to be a very cost-effective support system for short and medium span bridges. A typical pile cap using this system is shown in Figure 1. While the bent shown is for an intermediate bent, this research applicable to abutment caps as well. This type of system offers low initial cost, short construction time, low maintenance requirements, and a long service life. While the gravity load performance of these systems is well understood, their strength and ductility under extreme lateral loads (e.g., seismic events) is more difficult to reliably predict using conventional design procedures. This project aims to further develop newly established design and analysis methodologies to ultimately ensure bridge performance is fully consistent with design intent.


Figure 1: Typical MDT concrete-filled steel pile and concrete pile cap bridge substructure support system (Pryor Creek Bridge near Huntley, MT – courtesy of MDT (2012))

## 1.2 Objective and Scope

The primary objectives of this research were to (a) further validate/improve MDT's CFST to concrete pile cap connection design/analysis methodologies, (b) ensure the efficacy of these methodologies for a wide variety of potential design configurations, (c) gain further insights on the basic connection behavior under extreme lateral loads, and (d) determine possible improvements in the design methodology.

As mentioned previously, there are numerous benefits realized in using CFSTs in structural applications. To realize many of these benefits, however, the connections between CFSTs and other structural elements, such as pile caps and foundations, need to be designed and detailed to achieve the full moment demand on the connection. Therefore, it is essential to be able to reasonably predict the strength of the CFST and the behavior and capacity of the connection to the pile cap.

This report presents the results and subsequent conclusions from tests on four CFST-to-pile cap connections of various sizes, and with varying concrete strengths and reinforcing details. The four designs were chosen to exercise several parameters of the MDT design methodology. Specifically, this report begins with a brief literature review focused on recent studies performed on CFST pile cap connections. It then discusses details of the experimental program, including load setup, instrumentation, and specimen design and details. Results from the tests are then presented and discussed. The measured capacities from these tests are then compared to the predicted capacities obtained from the MDT design methodology, and the efficacy of this prediction methodology is evaluated. Finally, key findings are presented and discussed.

# 2 LITERATURE REVIEW

This literature review is focused on recent research aimed at better understanding the behavior/performance of CFST to pile cap/beam connections. Specifically, it focused on research that has been conducted since the completion of the previous phase of research [1].

## 2.1 Structural Behavior of Double-CFST Pile Foundations under Cyclic Loads

Li, Xiao [2] investigated the structural behavior of double CFST-Piles embedded in concrete pile caps subjected to seismic loads. Specifically, they tested vertical and battered piles under cyclic lateral loads, and documented the observed failure modes, ultimate strength, lateral stiffness, displacement ductility, and energy dissipation capacity of the specimens. A total of three double CFST-pile specimens with differing configurations were tested in this research, as shown in Figure 2. A finite element model was also calibrated and used to investigate the effects of varying embedment depth and inclination angle.

The vertical pile configuration was designed with embedment depth prescribed by Chinese structural codes, which specify a minimum embedment depth of 1.0 times the diameter of the CFST (D). This specimen ultimately failed due to block shear in the pile cap at the two free ends, after initial yielding of the CFST piles. Due to the block shear failure in the cap and separation between CFST piles, the plastic hinges in the CFST piles were not fully developed, resulting in a pinched hysteresis curve, and subsequently the lowest energy dissipation capacity. As expected, the ultimate capacity of this specimen was the lowest of three specimens, was the most flexible, and had the most ductile response.

The battered pile configurations experienced higher ultimate capacities and were significantly stiffer than the vertical-pile specimen. This is expected since a portion of the lateral load is carried by the axial component of the battered piles. Ultimately these specimens failed due to cracking, concrete pry out, and buckling of the CFST. It was observed that the loading capacity deteriorated rapidly at drift ratios higher than 6% due to concrete pry out of the pile cap, resulting in a lower deformation capacity. Additionally, relative to the vertical pile specimens, the battered piles were observed to have an increased energy dissipation capacity, and a reduction in ductility.

It was concluded that an embedment depth of 1.0D is adequate for forming plastic hinges at the ends of both vertical and battered CFST piles. However, it was observed that block shear failure and concrete pry-out at large drift ratios prevent the complete development of the plastic hinges. Modeling in ABAQUS validated this finding. Thus, an embedment depth of 1.5D is recommended for these connections to improve energy dissipation capacity. It was also concluded that the battered piles significantly increase the ultimate capacity, lateral stiffness, and energy dissipation capacity of the connections, but resulting damage reduces the deformation capacity and ductility. Regarding the effects of unequal pile heights, the shorter piles experienced increased shear and axial loads, resulting in the premature failure of the shorter pile. That being said, the ultimate lateral load carrying capacity of the connection was not significantly affected by the unequal heights, but the deformation capacity decreased with an increase in the ratio between heights.

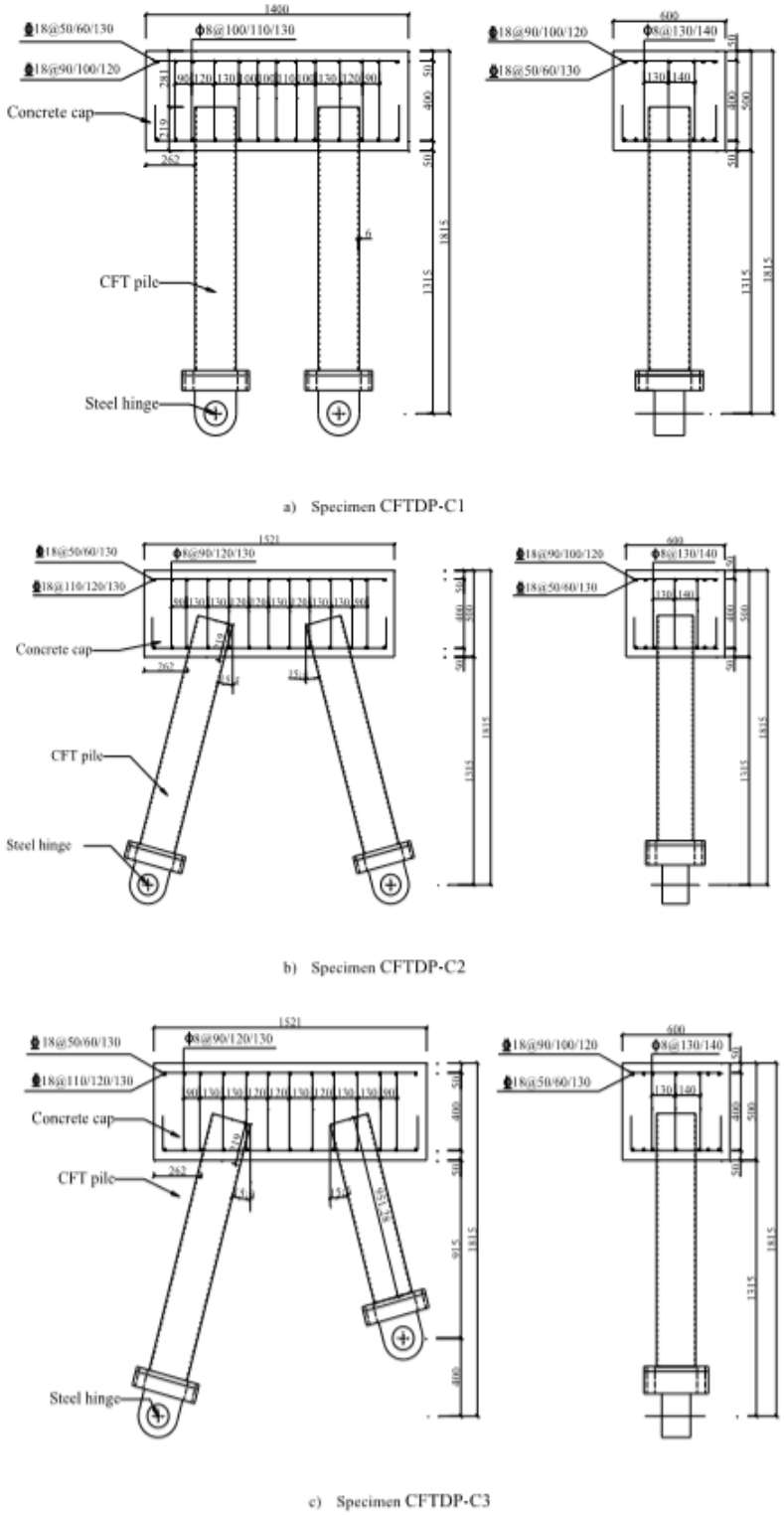


Figure 2: CFST Pile Configurations Tested by Li, Xiao [2]

## 2.2 Punching Shear in CFST Connections

The punching shear capacity of CFST to pile foundation connections was recently investigated [3]. While this behavior is relatively well understood for RC columns, CFST column to pile cap connections have more complicated load transfer mechanisms. As part of this research, five CFST column to pile cap specimens were tested under punching shear loads, and the effects of embedment depth, shear studs, face annular rings, and double-headed shear reinforcement were investigated. Each specimen consisted of a pile cap suspended by four CFST piles, shown in profile view in Figure 3. The contribution of soil below the piles was not considered in this study, and piles were placed on a rigid steel platform. Monotonic vertical loading was applied towards the floor with a hydraulic actuator, while measuring the applied loads, strains in the CFST columns and steel reinforcement, and center deflection of pile caps. An analytical study was also carried out using ABAQUS.

All five specimens failed due to punching shear, and the observed failure mechanisms were greatly affected by the connection details. The specimen with the face annular ring showed the highest load carrying capacity and exhibited the most ductile behavior, since the annular rings were able to increase the effective perimeter of the critical section for punching shear. All other tested specimens experienced brittle punching shear failure leading to a substantial drop in load-carrying capacity. The reduction of column embedment depth resulted in an increase in effective depth for the RC pile caps, leading to a significant increase in punching shear capacity of the connection. The headed shear reinforcement included in the pile cap also significantly increased the punching shear capacity of the connection. It was also concluded that current code predictions (AASHTO and ACI 318-14) for the punching shear capacity of CFST to pile cap connections are overly conservative, and thus an empirical model for predicting the punching shear capacity of CFST column to concrete-cap connections was developed and evaluated.

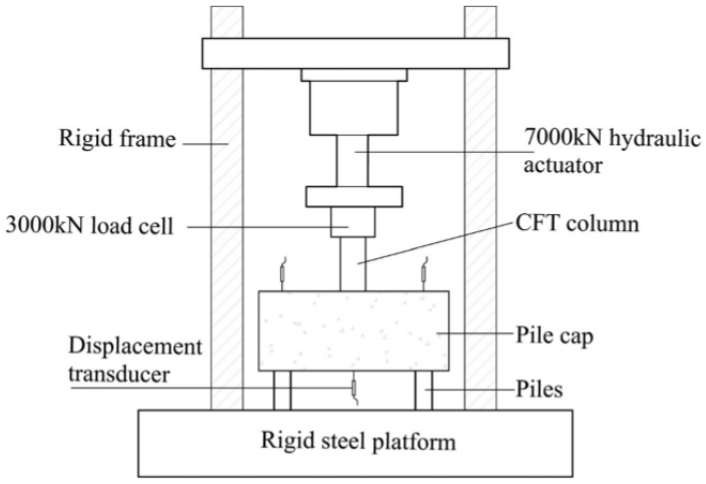


Figure 3: Punching Shear Test Setup [3]

## 2.3 University of Washington Studies

The University of Washington has conducted several research programs focused on investigating the structural performance of CFST's and their connections to concrete foundation caps/beams. Their investigation of the topic began in 2005 with the goal of understanding a foundation connection capable of developing the full plastic moment capacity of CFST piles. The early phases of research involved testing 19 half-scale CFST column-to-foundations connections [4-7]. These connections included flanged annular rings welded to the base of the CFSTs. These specimens evaluated the effects of various connection parameters (e.g., embedment depth, steel strength and connection type) on the performance of the CFST under seismic loading. Two variations of the embedded connection were developed and tested: a CIP monolithic option and a partial height pocket option. These tests were successful, resulting in full plastic hinging of the embedded CFSTs.

The early phases of research also investigated the behavior of the CFSTs independently from the connection. These studies included nonlinear finite element analyses of high strength CFSTs under flexural loading [8]. This modeling led to better understanding of CFST behavior, especially with respect to local buckling of the steel tube. Another notable research project was aimed at further understanding composite action in CFST components and connections [9]. Understanding and achieving the shear-stress transfer necessary for composite action is a significant obstacle in the optimal use of CFSTs. It was found that circular CFSTs develop composite action more readily than rectangular shaped piles. Achieving composite action with mechanical transfer using interior studs or rings may be necessary, but these are difficult to install. Additionally, it was concluded that base annular rings provide direct bearing between the embedded CFST and surrounding concrete, providing a mechanism to efficiently develop large bearing stresses.

Another project focused on modeling CFSTs under combined loading (including internal reinforcement), and evaluating and improving design provisions for such elements [10]. This research resulted in an improved P-M interaction curve for these elements and determined that current US design codes accurately predict performance under axial or bending load but are overly conservative at predicting behavior under combined loading.

The later phases of research have made progress in developing design expressions for CFST to foundation footing/beam connections subjected to lateral loads [11-17]. In this research, three column-to-cap connections subjected to cyclic deformations were studied, all of which had precast caps that included pockets for the embedded CFSTs. These pockets were formed by embedding corrugated pipes in the precast caps and were filled with high strength grout after the CFSTs were placed in the sockets. The connection types are illustrated in Figure 4. The embedded ring connection (ER) was similar to the connections studied in the previous research, and included an annular ring welded to the tip of the embedded CFST. This connection detail resulted in large ultimate strengths, high stiffnesses, and large deformation capacities. In testing, local buckling was observed in the steel tube at drifts in between 1.5-3%. However, the buckling did not influence the stiffness or moment resistance of the connection [14]. Testing showed full plastic moment capacity was achieved for decreased annular ring widths of D+16t and cap widths as low as 2D. The ER connection was concluded to have superior seismic performance and accelerated bridge construction (ABC) compatibility in comparison to the other connection types.

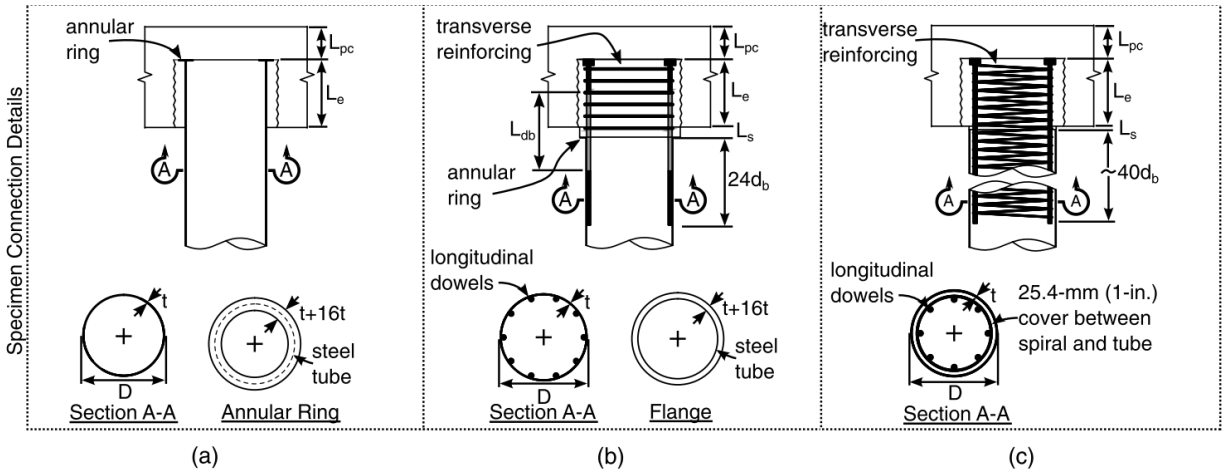


Figure 4: Connection Types Investigated in Later Phases of UW Research: (a) ER connection; (b) WD connection; (c) RC connection [12]

The second connection option studied was the Welded Dowel (WD) connection. This connection implements a ring of headed dowels to resist flexural demand. To maximize moment capacity, the dowel is welded directly to the tube. An outer diameter of D+8t is used and welded to the exterior of the tube. When tested, the connection exhibited large strength, stiffness, and deformation capacity. However, comparable ER connections exhibited higher stiffness and strength. The stiffness and strength of the WD connection is controlled by the effective reinforcing ratio of the dowels which extend into the cap beam. Furthermore, the WD connection has several disadvantages in terms of labor efficiency and ABC. Temporary shoring is required, and dowels must be welded to the inside of the tube, which is labor intensive.

The final connection investigated was an RC connection in which the CFST was terminated at the surface of the cap/beam. Experimental results suggest that this connection type exhibits significantly lower strength and stiffness in comparison to a CFST component. This was because stiffness and strength are controlled by the effective longitudinal reinforcing ratio in the connection. Yielding and fracture of the longitudinal reinforcing were observed to be the primary failure mechanisms. This method was also labor intensive and required the construction of a reinforcing cage that must be temporarily supported within the steel tube. When comparing all three connections, the ER option was observed to have superior ABC facilitation and seismic performance.

This research included developing and validating a numerical model in ABAQUS [12, 17]. Due to the complexities associated with modeling the nonlinear cyclic behavior of the ER connection, prior numerical efforts have focused primarily on monotonic behavior and failure envelopes rather than cyclic behavior. The model developed in this research aimed to capture the nonlinear cyclic behavior of the ER connection including the composite interaction between the materials. A key component to this modeling strategy was numerically "pre-cracking" the concrete fill. When compared to test data, this modeling strategy was shown to accurately predict damage and overall behavior of the elements.

Finally, a case study was performed to evaluate and quantify the performance of CFST bridges in comparison to RC bridges [12, 16]. Reinforced concrete is commonly used for bridge construction in

seismic regions because of its stiffness, strength and inelastic deformation capacity [16]; however, RC bridges require special detailing in regions of plastic hinging as mandated by AASHTO Guide Specifications [16]. Unfortunately, these detailing requirements often result in congested reinforcing that deters ABC and increases cost. On the other hand, CFST connections can achieve the plastic moment capacity of the pile without the use of internal reinforcing in the pile. Further, it has been demonstrated that, for a given strength, the diameter of a CFST column is 20-40 percent smaller than an RC column [16]. This brings weight and materials savings. To compare the performance of CFST and RC bridge structures, several nonlinear modeling approaches were introduced. An RC bridge was redesigned using CFST columns and inelastic modeling was used to conduct the comparison case study. It was found that the CFST structure exceeded the performance of the RC structure for all hazards in the *Multiple Seismic Hazard Analysis* [16]. Furthermore, the drifts seen in the CFST structure remained below the threshold that would require repair, while the RC structure exceeded the threshold warranting repair. Relative to the CFST structure, it was found that the RC structure has a higher probability of *Repair Required, Partial Replacement,* and *Collapse/Replacement* scenarios for lower spectral accelerations. Overall, the CFST was shown to be a more efficient bridge structure in seismic regions.

It should also be noted, that the above research has resulted in a design procedure that has been recently adopted by the Washington Department of Transportation [18].

## 2.4 Previous Research at Montana State University

MDT has sponsored previous research at Montana State University (MSU) to investigate the performance of CFST piles under extreme lateral loads and to develop appropriate analysis/design procedures [1, 19-21]. As part of these investigations, MSU conducted physical tests on various half-size models of the CFST to pile cap connections under pseudo-static and cyclic loading (

Figure 5 and Figure 6). While this research provided useful information regarding the behavior and design of CFST to concrete pile-cap connections and led to a new analysis methodology [22], additional research is required to further characterize this behavior more fully develop the new analysis methodology. For example, several aspects of this methodology rely on empirical assumptions that may not be valid for all possible cap configurations. That is, the tests carried out in the previous research did not vary cap dimensions, CFST diameter, or loading configuration; therefore, the new analysis methodology may not be valid for all conditions. Thus, further testing and/or analytical modeling is needed to validate and possibly modify these elements of the proposed methodology to ultimately ensure the desired system performance.

Figure 5: Typical Test Specimen from Previous MSU Research

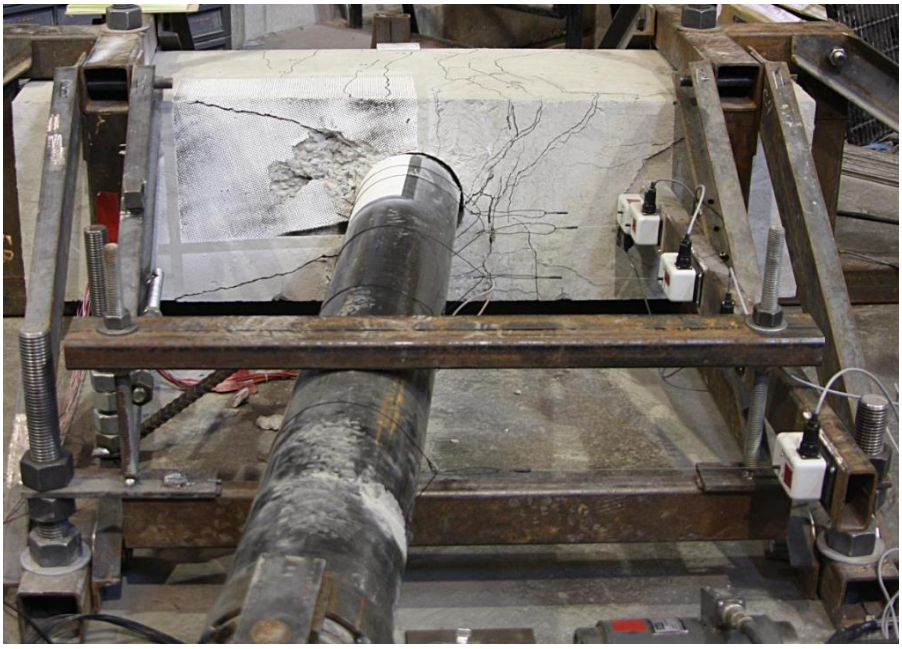

Figure 6: Typical Test Specimen from Previous MSU Research Near Ultimate Load

# 3 EXPERIMENTAL DESIGN

## 3.1 Overview

The MDT CFST connection design/analysis methodologies rely heavily on empiricism and may not be valid for all cap configurations/dimensions. The current methodologies and the research that led to them were thoroughly analyzed to identify potential shortcomings that need to be addressed with further testing. An experimental program was developed to address the shortcomings identified in this analysis. Specifically, the proposed experimental design varied load setup (testing specimens vertically rather than on their sides), specimen scale, and reinforcement details relative to the original experiments. The results from this test series will be used to further establish the efficacy of the MDT design/analysis methodologies.

A total of four specimens were designed and tested in this research. The first specimen was a half-size specimen, which provided continuity between this and the previous test series, where all specimens tested were half-size. This specimen was lightly reinforced and represented a typical MDT connection design for use in situations where the lateral demand is not expected to control the design. The research then progressed to a 2/3$^{rd}$-size specimen with similar reinforcement to isolate any potential effects associated with specimen scale. The third specimen was the same size and had the same reinforcing scheme as the second specimen but had a higher strength concrete to isolate the effect of concrete strength. The final specimen was also identical to the second specimen but isolated the effect of including U-bars in the reinforcing scheme.

This chapter provides details on the test setup and instrumentation used in this research and provides the dimensions and reinforcing details for all specimens.

## 3.2 Test Setup, Instrumentation, and Loading Scheme

The test specimens consisted of a single connection from an overall bridge bent, as illustrated in Figure 7. Each specimen consisted of a portion of the pile cap (spanning halfway between consecutive piles) and a portion of the CFST pile (extending out of the pile cap to an assumed inflection point along its length). The specimens were supported and loaded in such a way as to generate the deflected shape expected in this subsection of the full-size bent (as illustrated by the dashed line in Figure 7).

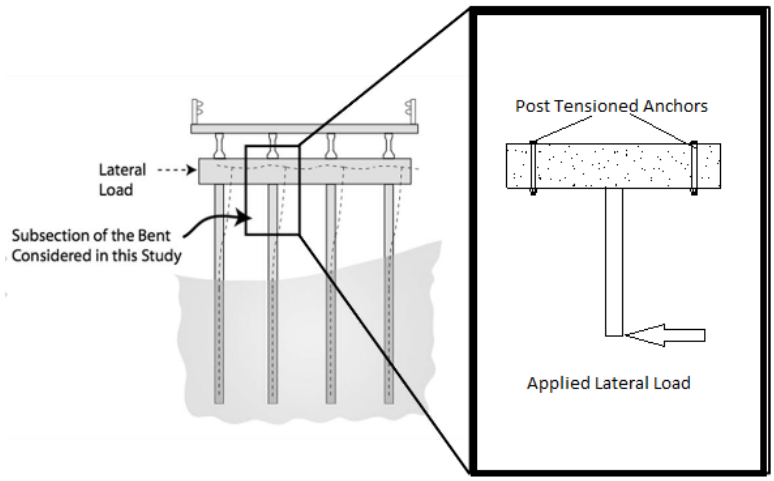


Figure 7: Subsection of CFST-concrete bridge bent

The specimens were tested in the Structure Lab housed in the Civil Engineering Department at MSU. The idealized test setup for the half-size specimen is shown in Figure 8, while the test setup for the 2/3$^{rd}$ -size specimen is shown in Figure 9. Photos of the actual load setups are provided in Figure 10 and Figure 11 for half-size and 2/3$^{rd}$-size specimens, respectively. In this phase of research, the test specimens were inverted and tested vertically, as shown. The concrete pile caps were post-tensioned to the strong floor, and a hydraulic actuator (reacting against the anchored load frame) applied a lateral load to the tip of the CFST, as indicated. The pile cap specimen was sitting on rubber pads at the location of the tie downs to allow for pile cap to rotate globally during testing. This loading scheme varies from the scheme used in the previous phases of research where the specimens were tested horizontally on their sides. This variation was made to investigate any potential effects that may have been attributed to the previous test setup. It should also be noted that lateral bracing was included near the tip of the CFST to inhibit any out of plane bending (as shown in Figure 10 and Figure 11).

The specimens were loaded monotonically until failure, at which point the load was reversed and the specimens were loaded to failure in the opposite direction and then returned to zero. The applied load and resultant displacements were monitored throughout testing. Displacements were monitored using string potentiometers mounted to an isolated frame at multiple locations along the height of the specimen, as indicated in Figure 8 and Figure 9. The load was measured using a load cell attached to the end of the hydraulic actuator. The testing was paused every 3,000 pounds of applied load to record any observable damage and take pictures. Black markers were also used to trace cracks so that they were observable in the photos.

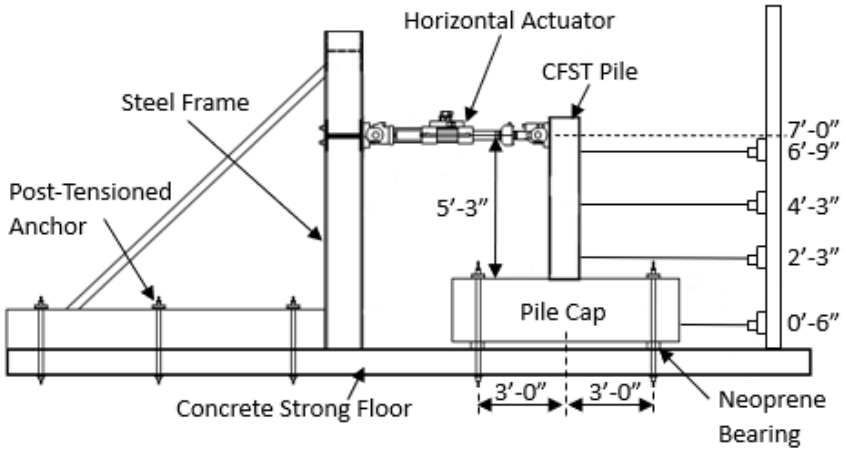


Figure 8: Test setup for half-size specimen

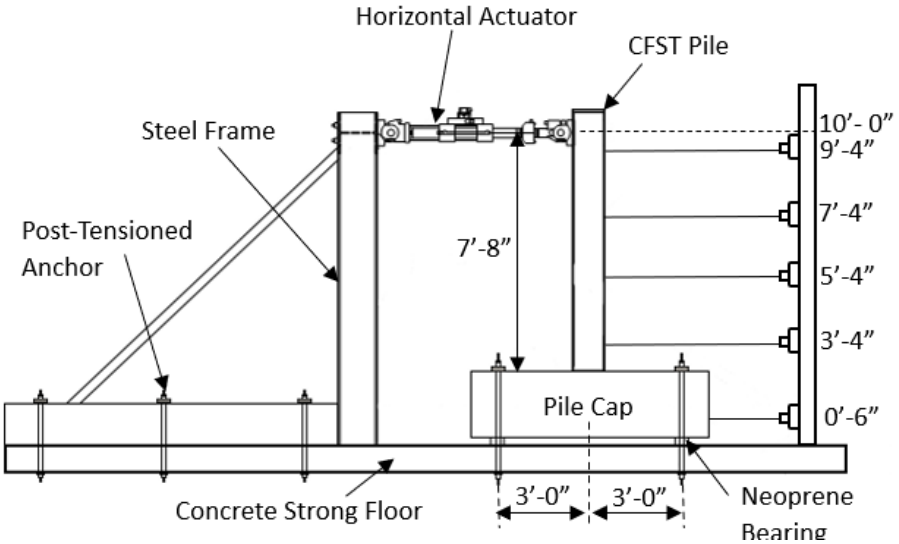


Figure 9: Test setup for 2/3-scale specimen

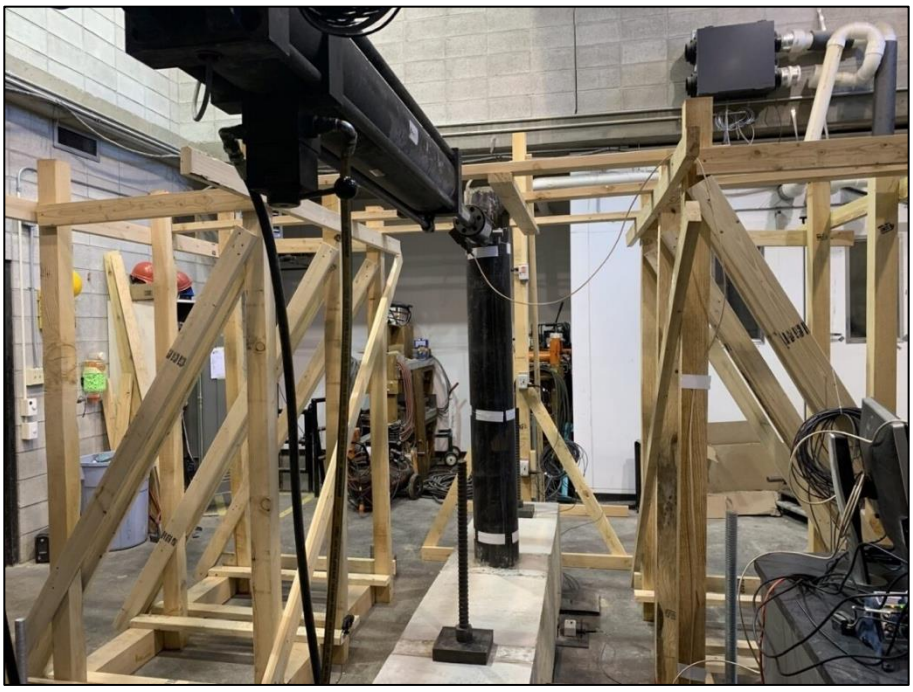

Figure 10: Actual half-size test setup

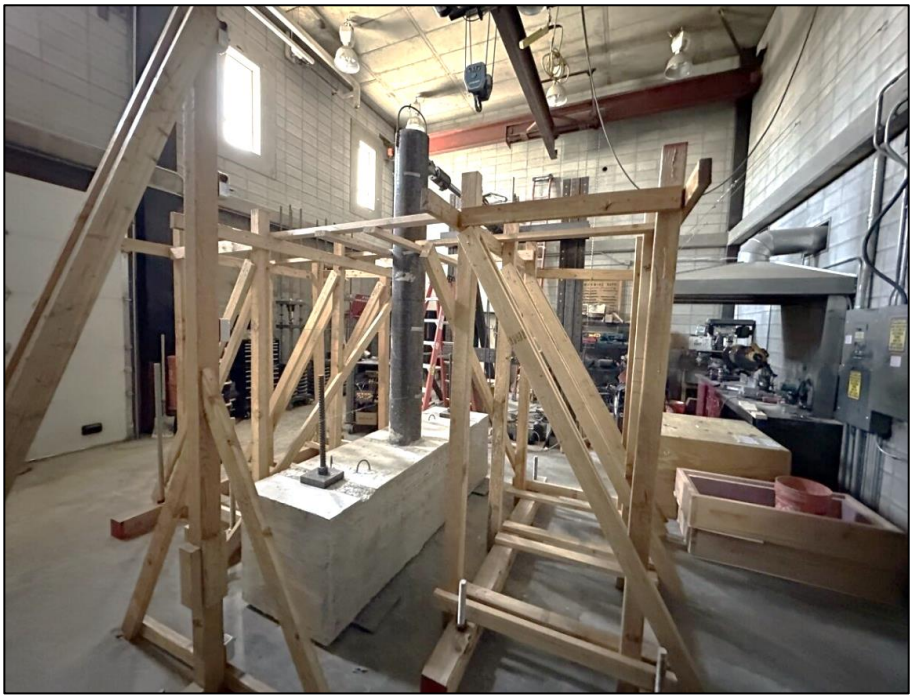

Figure 11: Actual 2/3rd -size test setup

## 3.3 Specimen Design

The test specimens were scaled from the MDT Standard Minimum design, which is lightly reinforced and is used in situations where the lateral demands are not expected to control the design of the connection. The structural drawings (from a typical bridge project) of this Standard Minimum connection are provided in Figure 12. A full-size test specimen based on this Standard Minimum Design is shown in Figure 13. Note that this full-size specimen was not tested in this research but is provided here to assist in demonstrating the scaling process. This connection design consists of longitudinal reinforcement spanning along the length of the pile cap and is included to help carry the loads induced within the pile connection and to carry the global bending moments. Transverse reinforcement is included along the length of the cap to provide shear resistance and confinement. Note that the transverse reinforcement is more tightly spaced around the pile connection to provide additional confinement in this region, and because the global shear demand is greater in this region. In this design, the CFST is embedded to mid-depth of the cap.

The test specimens in this research were scaled from the full-size configuration (Figure 13). Specifically, the dimensions were scaled-directly from the full-size specimen, as were the general locations and approximate amount (as a percent of the concrete volume) of reinforcing steel. The minimum spacing between rebar was also considered during the scaling process. It should be noted that, due to testing configuration limits (governed by the location of strong-floor holes), all specimen caps were 8-ft long, and had a clear span between post-tensioned tie downs of 6 ft. For convenience, each specimen was named in a way that would convey the size, target concrete strength, and reinforcing scheme. “Verification test” was abbreviated to VT at the beginning of each name. This was followed by the size of the specimen. The target concrete strength was denoted using the strength of the concrete in ksi. Finally, a “U” at the end means that the specimen had U-bars. For example, the first specimen was called VT1/2-4, meaning that it was half-size with 4 ksi target concrete strength and had no U-bars. The following sections discuss each of the four test specimens in detail.

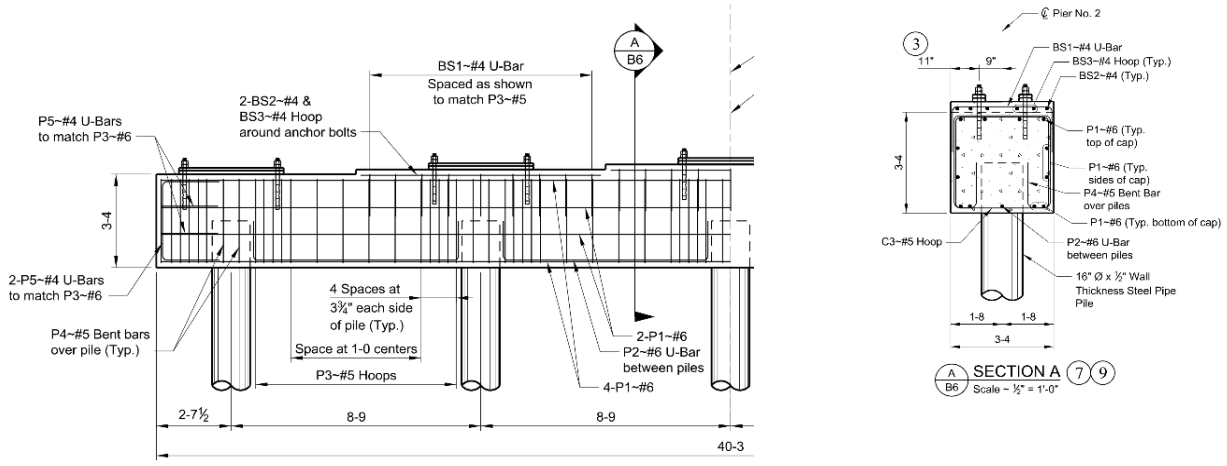


Figure 12: MDT Standard Minimum cap design

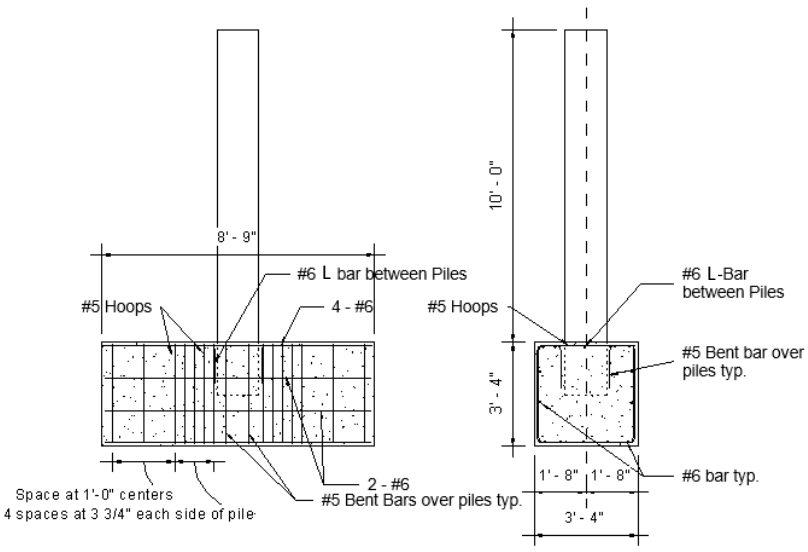


Figure 13: Full-size test configuration

### 3.3.1 Specimen 1 Design – VT1/2-4

As stated above, the first test specimen was a half-size version of the full-size connection discussed above. The concrete cap in this specimen was 20 inches by 20 inches, and 8 feet long. It included #4 longitudinal reinforcement along its length, as shown. The transverse reinforcement consisted of #3s spaced at 6 inches in the regions away from the connection, and #4s spaced at 2-1/2 inches in the region of the connection. The CFST pile had an outside diameter of 8-5/8 inches, and a wall thickness of ½ inch. The rebar was Grade 60, and the CFST pipe was A53 Grade B steel with a specified yield stress of 35 ksi. The concrete was a standard commercial mix supplied by Quality Ready Mix in Bozeman, Montana. The concrete strength on the day of testing was 4000 psi.

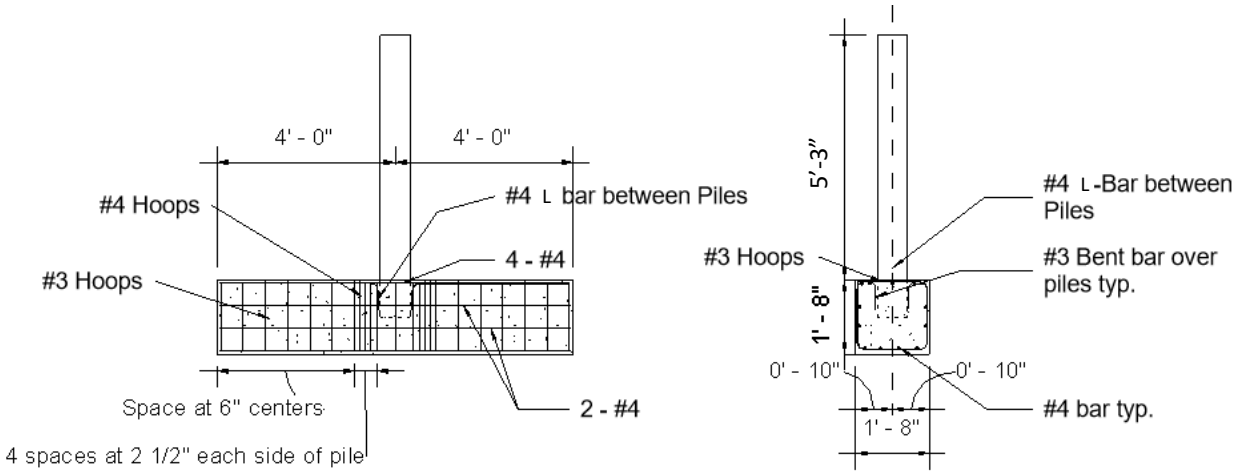


Figure 14: Half-size test configuration

### 3.3.2 Specimen 2 Design – VT2/3-4

The second specimen was a 2/3rd-size version of the Standard Minimum Design. The concrete cap in this specimen was 27 inches by 27 inches, and 8 feet long. It included #5 rebar longitudinal reinforcement along its length and #4 transverse reinforcement. The transverse spacing was 8 inches in the regions away from the connections, and 2-1/2 inches in the region of the connection. The CFST pile had an outside diameter of 10-3/4 inches, and a wall thickness of ½ inch. The rebar was Grade 60, and the CFST pipe was A500 Grade B steel with a specified yield stress of 42 ksi. The concrete was a standard commercial mix supplied by Quality Ready Mix in Bozeman, Montana. The concrete strength on the day of testing was 4000 psi.

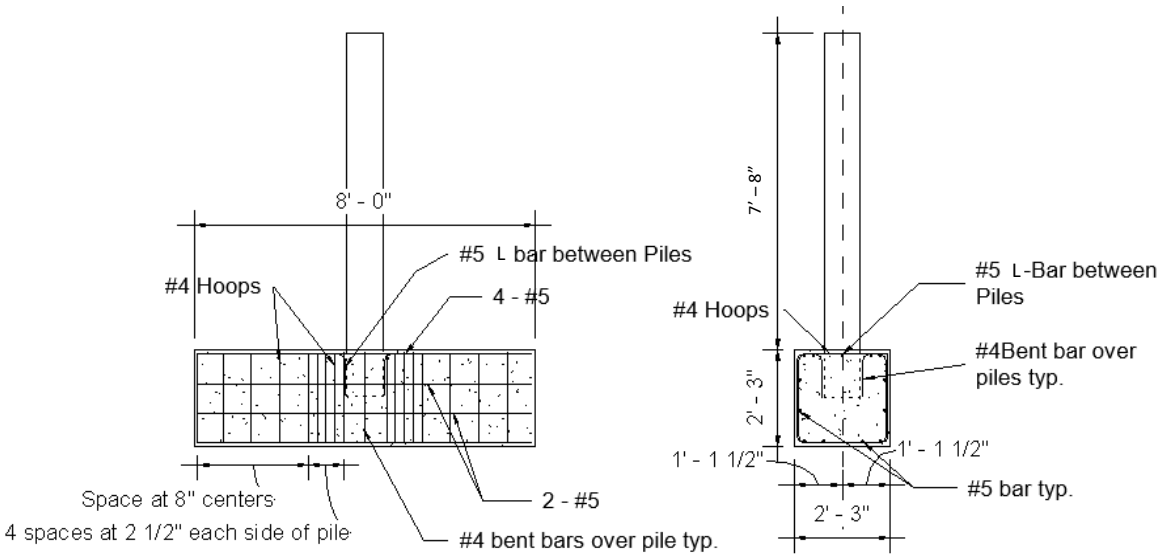


Figure 15: 2/3rd-size test configuration

### 3.3.3 Specimen 3 Design – VT2/3-6

The third specimen was the same as the second specimen with the exception of the target concrete strength (6 ksi vs 4 ksi). That is, this specimen had the same cap dimensions, reinforcing scheme and strengths, and used the same size CFST with the same specified strengths. It should be noted that the concrete strength plateaued at around 5500 psi, and therefore this was the strength on the day of testing. Again, Quality Ready Mix out of Bozeman, Montana was the provider for this concrete.

### 3.3.4 Specimen 4 Design – VT2/3-4U

The final specimen used the same size CFST pile, the same cap dimensions, and the same general reinforcing scheme as the previous two tests but included U-bars at several locations around the tip of the embedded pile. There were four #6 U-bars in total, two (one each direction) near the connection face approximately 2 inches below the concrete, and the other two near the embedded tip approximately 1-1/2 inches from the end of the pile, as shown in Figure 17. The target concrete strength was 4000 psi but was 4800 psi on the day of testing. As before, Quality Ready Mix in Bozeman, Montana provided the concrete for this specimen. Figure 16 shows the U-bar reinforcement.

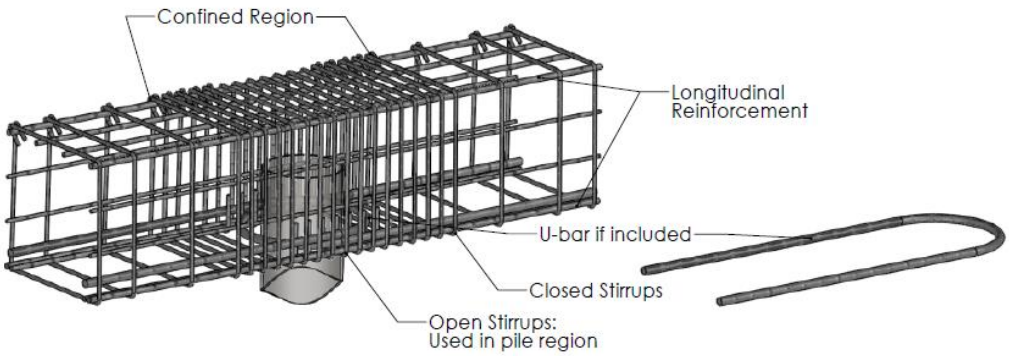


Figure 16: Typical U-bar reinforcement

Figure 17: U-Bar placement in VT2/3-4U

## 3.4 Specimen Construction

The construction of each specimen began with tying the rebar cage, as shown in Figure 18. It should be noted that the rebar stirrups and U-bars were prepared by Concrete Connections out of Bozeman, MT.

Once tied, the rebar cage was then placed into the formwork, which was constructed with dimensional lumber and ¾-inch plywood, as shown in Figure 19. The holes for the post-tensioning rods were constructed with 2" PVC pipes that extended through the pile cap. After placing the cage within the formwork, the CFST pile was then lifted into place and held plumb by A-frames attached to either side of the formwork, as shown in Figure 19.

Figure 18: Reinforcing cage under construction

Figure 19: Full specimen setup before concrete pour

After placing the CFST, concrete was then placed into the forms and the CFST (Figure 20). The cap was filled first, then the CFST pile was filled from the top using 5-gallon buckets, as shown in Figure 21. The concrete was vibrated during placement to ensure proper consolidation. Concrete cylinders were cast for compression testing throughout the pour, as shown in Figure 22. After finishing the concrete, rebar pick points were inserted into the top of the finished surface of the cap to provide a mechanism to move the specimen into place with the overhead crane after curing. Upon completion, the specimen was covered with plastic to keep moisture from evaporating during the curing process, as shown in Figure 23.

Figure 20: Filling the cap from concrete truck chute


Figure 21: Filling CFST with Concrete

Figure 22: Casting concrete cylinders

Figure 23: Specimen upon completion of concrete pour

## 3.5 Cylinder Curing & Testing

The concrete cylinders were tested in compression following procedures specified in ASTM C39. Cylinders were tested every day until the target compressive strength was reached or until the strengths plateaued. Most of the cylinders were cured in a standard moist cure room, while several were field cured next to the pile cap specimen. The field-cured specimens were tested on test day to provide more information on the actual concrete strength of the specimen.

# 4 TEST RESULTS

The results of the monotonic tests conducted on the four CFST pile-to-concrete pile cap connections described in Chapter 3 are reported in this chapter. An overview of the important parameters characterizing each test along with the corresponding test results is presented in Table 1. Referring to this table, significant items that varied between tests are concrete specimen size, concrete strength, and the inclusion of U-bar reinforcement. The results from each specimen are discussed in detail in the following section. In these sections, the applied moment was calculated as the measured load multiplied by the distance from the top of the cap (in the testing position) to the application of the lateral load at the assumed inflection point. The drift was determined from the highest placed displacement gage, and calculated as the measured displacement from this gage divided by the distance from the top of the pile cap to the location of the gage.

Relative to general performance, the first three specimens failed due to concrete crushing and cracking within the pile cap at moments of 101.5 k-ft, 208.3 k-ft, and 276.7 k-ft, respectively. The fourth specimen, failed due to the formation of a plastic-hinge at the base of the CFST at a moment of 332.3 k-ft.

The results of each of the tests are presented in more detail in the following sections.

Table 1: Summary of test results

| Specimen Name | Concrete Strength (psi) | Specimen Scale | Reinforcing Scheme | Failure Mechanism | Ultimate Moment (k-ft) |
|---|---|---|---|---|---|
| VT1/2-4 | 4000 | 1/2 Scale | Normal | Cap Failure/Crushing Cracking | 101.5 |
| VT2/3-4 | 4000 | 2/3 Scale | Normal | Cap Failure/Crushing Cracking | 208.3 |
| VT2/3-6 | 5500 | 2/3 Scale | Normal | Cap Failure/Crushing Cracking | 276.7 |
| VT2/3-4U | 4800 | 2/3 Scale | U-Bars Added | Plastic Hinge in CFT | 332.3 |

## 4.1 Specimen 1 - VT1/2-4

The first specimen was a half-size version of MDT Standard Minimum design and had a concrete strength of 4 ksi. This specimen was intended to provide continuity between this test series and the previous series, which tested half-size specimens horizontally.

The measured moment-drift response for this specimen is shown in Figure 24, and the first pull is isolated in Figure 25. As shown in the figures, the tip of CFST pile was pulled in one direction until failure was evident, after reaching a maximum moment of 101.5 k-ft. The tip of the pile was then returned to zero drift, and then pushed in the opposite direction until the cap had failed in this direction, after reaching a maximum moment of 87.4 k-ft. The tip of the pile was then returned to zero drift. Note the expected pinched hysteresis response due to the lack of fixity from the extensive damage in the cap during the pull cycle. Also note that the ultimate capacity obtained in the push direction was only 86% of that obtained on the initial pull cycle.

Regarding observable damage, the CFST remained elastic throughout testing, showing no signs of damage. However, as expected, the cap showed significant signs of damage throughout testing. The first cracks in the cap were observed at a moment of approximately 47.3 k-ft, propagating halfway down each side of the

pile cap as shown in Figure 26. This cracking is also observable in the moment-drift curve (Figure 25), marked by the slight change in stiffness at this moment. At 63 k-ft, a gap began to form on the backside of the pile and cracks started forming at 45-degree angles from where the pile was bearing on the cap as shown in Figure 27. The gap on the opposite side of the pile continued to increase as the load and displacements increased. The specimen reached an ultimate moment of 101.5 k-ft, at which point the load carrying capacity began to decrease. The failure was determined to be due be a combination of (1) concrete crushing on the bearing side of the pile and on the backside of the pile near the tip of the embedded pile, (2) tension cracks on the backside of the pile that extended the full height of the specimen (Figure 28), and (3) concrete near the surface of the pile prying up (Figure 28 and Figure 30). Figure 29 shows the specimen at failure in the push direction.

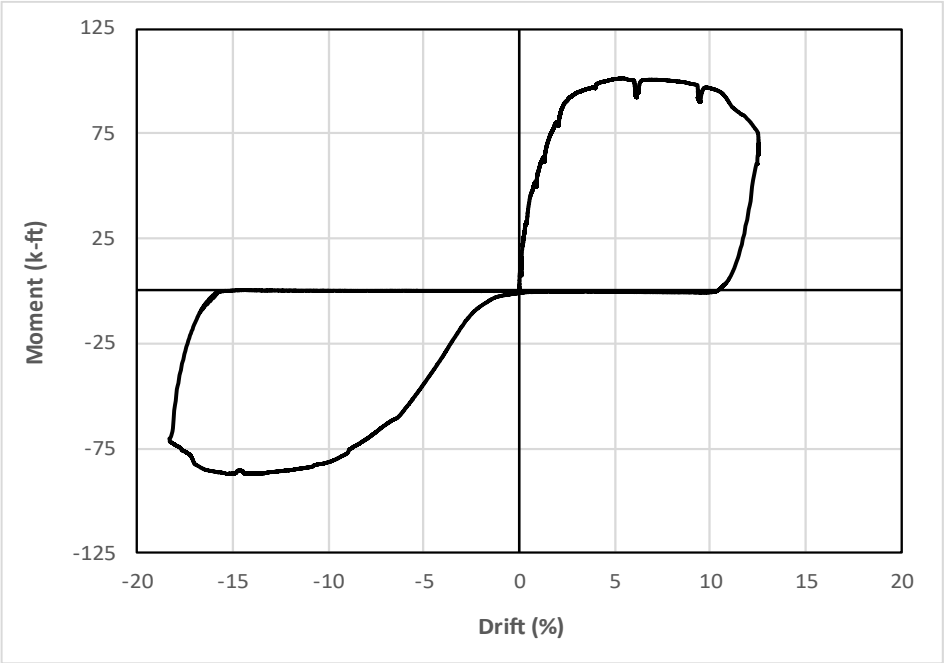


Figure 24: VT1/2-4 moment-drift relationship

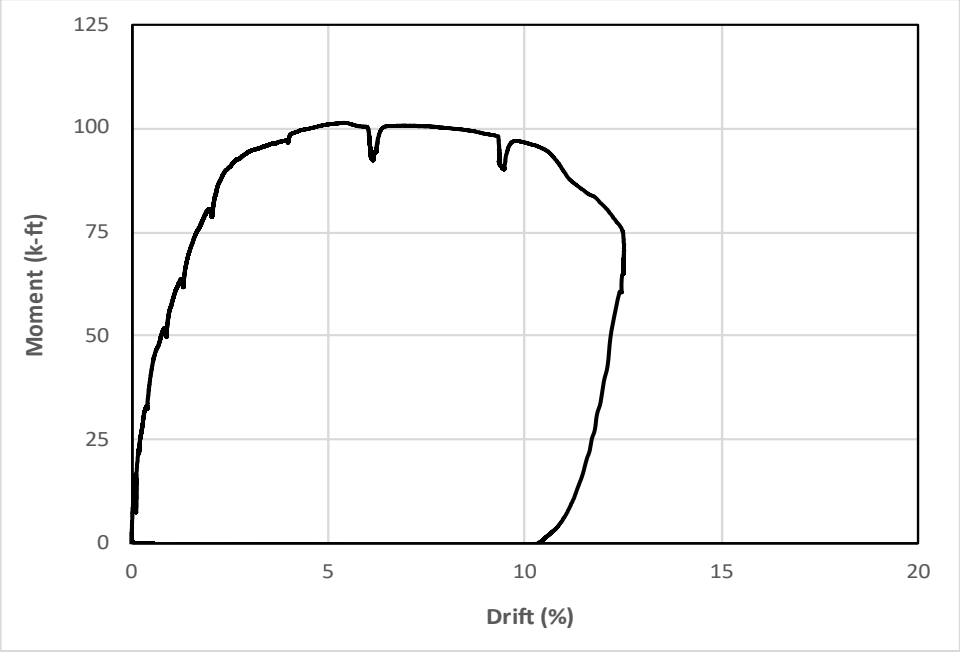


Figure 25: VT1/2-4 moment-drift relationship (first pull)

Figure 26: VT1/2-4 first cracks (47.3 k-ft)

Figure 27:VT1/2-4 45-degree cracks (63 k-ft)


Figure 28: VT1/2-4 failure from initial loading direction


Figure 29: VT1/2-4 failure from reverse loading direction

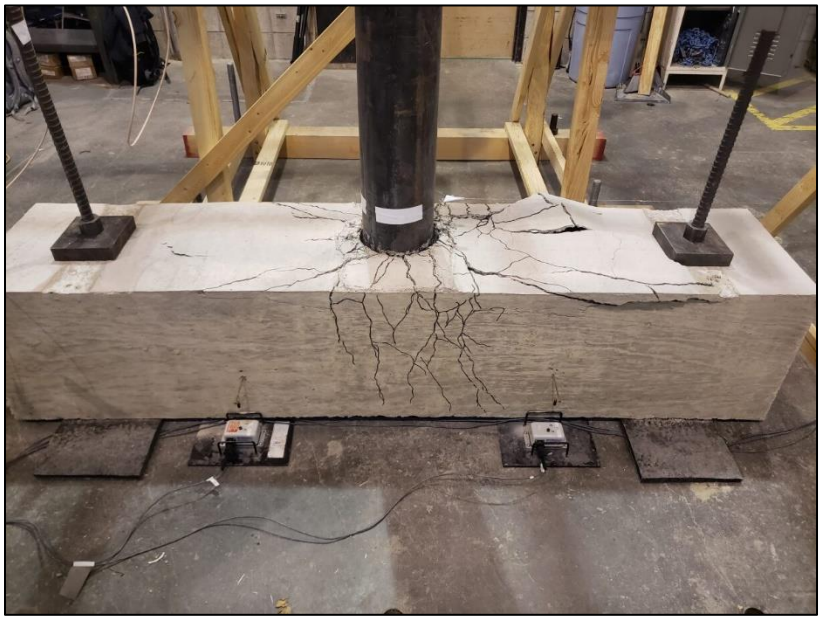

Figure 30: VT1/2-4 prying action on back side of pile cap

## 4.2 Specimen 2 - VT2/3-4

The second specimen, VT2/3-4, had the same basic design and concrete strength as the first specimen, but was 2/3rd-size rather than half-size. This was done to isolate the effects of size on connection performance.

The full measured moment-drift curve for this specimen is provided in Figure 31, while the curve from the first pull is highlighted in Figure 32. As shown in these figures, the CFST pile tip was pulled in one direction until a drift of around 18.5%, after reaching an ultimate moment of 208.3 k-ft. The load was then reversed, and the specimen was pushed in the opposite direction till failure, after reaching a maximum moment of 192.2 k-ft. The tip of the pile was then returned to zero drift. Again, note the expected pinched hysteresis response due to the lack of fixity from the extensive damage in the cap during the pull cycle. Again, the ultimate capacity in the push direction was only 92% of that obtained on the initial pull cycle.

Regarding observable damage, the initial cracks in the cap were observed at a moment of around 69 k-ft (Figure 33). At a moment of 115 k-ft, the pile cap had cracks that extended nearly the full depth of the specimen, and 45-degree angle cracks were observed to propagate across the top of the cap, as shown in Figure 34. Failure was determined to be due be a combination of (1) concrete crushing on the bearing side of the pile and on the backside of the pile near the tip of the embedded pile, (2) tension cracks on the backside of the pile that extended the full height of the specimen (Figure 35 and Figure 36), and (3) 45-degree angle cracks propagating along compression struts originating from the pile to the edge of the cap. Note that a gap was again formed on the backside of the pile (Figure 37), indicating a loss of fixity of the connection. The gap began forming at a moment of 92 k-ft and progressed until it was over 1” at the point of failure. The specimen at the extreme lateral deflection in the push direction is shown in Figure 38.

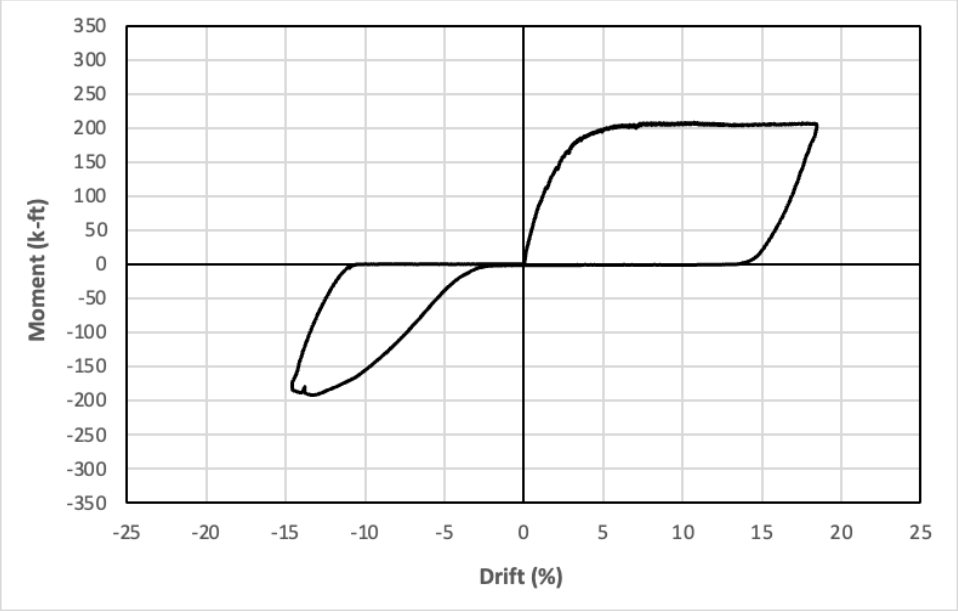


Figure 31: VT2/3-4 moment-drift curve

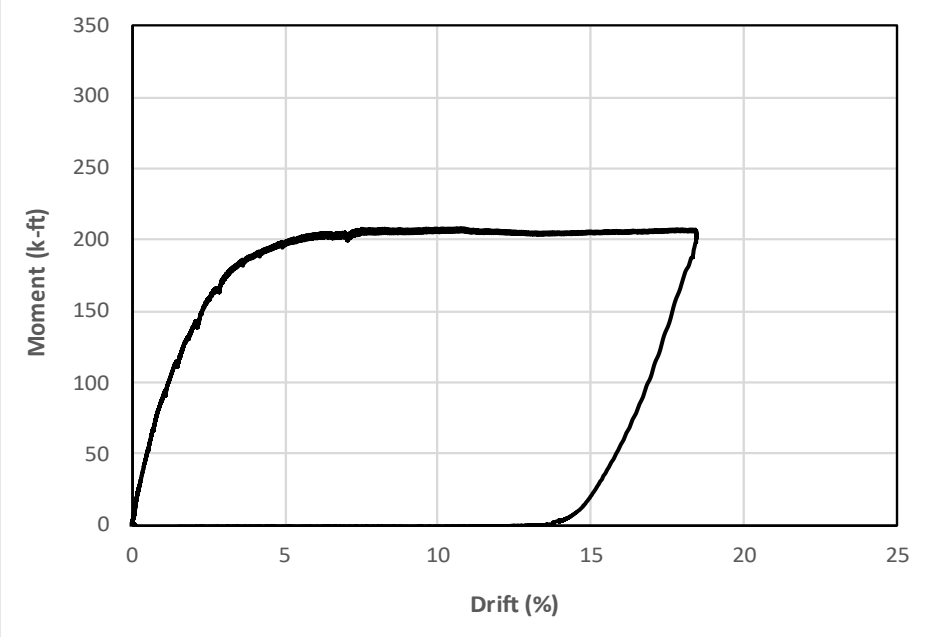


Figure 32: VT2/3-4 moment-drift curve (first pull)

Figure 33: VT2/3-4 first cracks (69 k-ft)

Figure 34: VT2/3-4 45-degree cracks (115 k-ft)

Figure 35: VT2/3-4 failure from initial loading direction

Figure 36: VT2/3-4 concrete crushing on front of pile at failure from initial loading direction

Figure 37: VT2/3-4 gap on back side of pile at failure from initial loading direction

Figure 38: VT2/3-4 failure from reverse loading direction

## 4.3 Specimen 3 - VT2/3-6

The third specimen, VT2/3-6 was identical to the second specimen with the exception of the concrete strength on the day of testing. This specimen was intended to have a concrete strength of 6 ksi on test day rather than the 4 ksi used in VT2/3-4, isolating the effect of concrete strength on connection performance. However, this specimen only obtained a concrete strength of 5.5 ksi on the day of testing.

Again, the full measured moment-drift curve for this specimen is provided in Figure 39, while the curve from the first pull is highlighted in Figure 40. As shown in these figures, the CFST pile tip was pulled in one direction until a drift of around 17.9%, after reaching an ultimate moment of 276.8 k-ft. The load was then reversed and pushed in the opposite direction until the actuator ran out of stroke, after reaching a moment of 229.6 k-ft. Note that at this displacement the cap had not yet reached its ultimate capacity in this direction. The tip of the pile was then returned to zero. Again, note the expected pinched hysteresis response due to the lack of fixity from the extensive damage in the cap.

As for damage, this specimen had a similar progression to that observed for the first two specimens. The first cracks were observed in the cap at a moment of 92 k-ft (Figure 41), significantly higher than that observed for VT2/3-4 (69 k-ft), most likely attributed to the increased concrete strength in this specimen (Figure 41). Similarly, the propagation of the cracks through the cap and the formation of 45-degree angle cracks along the compression struts did not become extensive until a load of around 138 k-ft (Figure 42). Again, failure of the cap was determined to be due be a combination of (1) concrete crushing on the bearing side of the pile and on the backside of the pile near the tip of the embedded pile, and (2) tension cracks on the backside of the pile that extended the full height of the specimen (Figure 43). Note that the 45-degree angle cracks are not as evident in this specimen as they were in the previous tests. Again, a gap was formed on the backside of the pile (Figure 43), indicating a loss of fixity of the connection. The gap began forming at a moment of 115 k-ft, a slightly larger moment than that VT2/3-4. The specimen at the extreme lateral deflection in the push direction is shown in Figure 38.

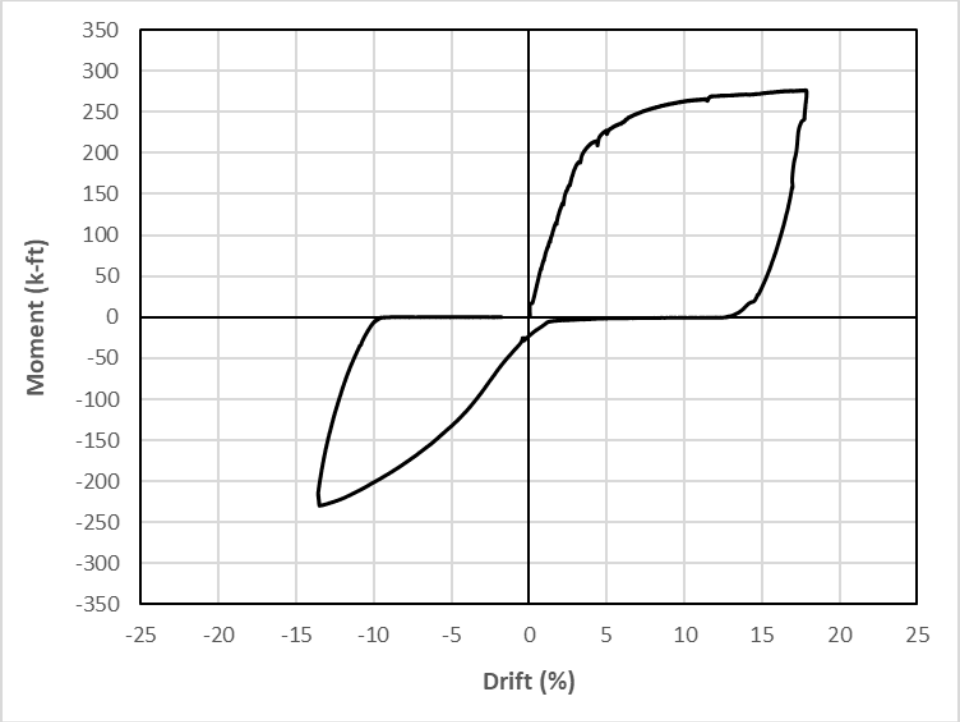


Figure 39: VT2/3-6 moment-drift curve

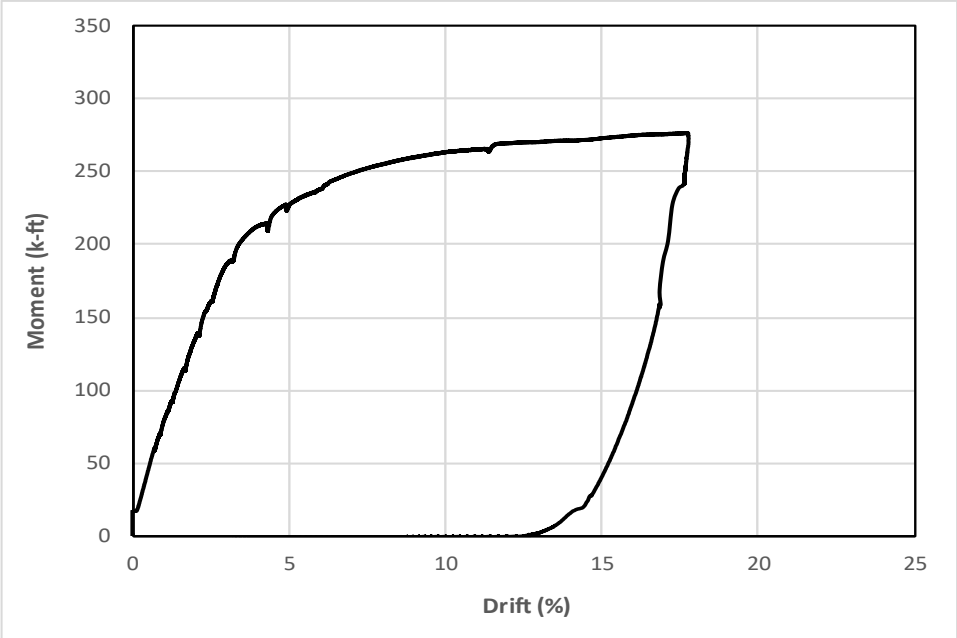


Figure 40: VT2/3-6 moment-drift response (first pull)

Figure 41: VT2/3-6 first cracks (69 k-ft)

Figure 42: VT2/3-6 45-degree cracks (138 k-ft)

Figure 43: VT2/3-6 failure from initial loading direction

Figure 44: VT2/3-6 failure from reverse loading direction

## 4.4 Specimen 4 – VT2/3-4U

The fourth specimen was identical to the second specimen but included U-bars embedded in the cap encircling the pile at two locations (the tip of the embedded CFST and near the surface of the cap). This test was designed to isolate the effect of U-bars on connection performance. It should be noted that the target concrete strength was 4 ksi, but this specimen was tested at a concrete strength of 4.8 ksi because testing was delayed due to issues with the loading mechanism. Therefore, some of the differences in performance may be attributed to U-bars and increased concrete strength.

The full measured moment-drift curve for this specimen is provided in Figure 45, while the curve from the first pull is highlighted in Figure 46. The behavior of this specimen is significantly different from that observed in the previous specimens because this specimen failed due to the

formation of a plastic-hinge in the CFST rather than failure of the cap (Figure 50). This was due to the increased strength of the connection due to the inclusion of the U-bars (and in some capacity due to increased concrete strength). This is the desired performance of this type of connection in high seismic regions due to the robust hysteresis response (non-pinched) and the resulting increase in energy dissipation capacity. The specimen was displaced to a drift of over 20% and the specimen's load carrying capacity was still increasing. At this drift, at a moment of 332.3 k-ft, the load was reversed because the actuator was out of stroke. During the reverse loading, the cap capacity was again sufficient to force the formation of a plastic hinge in the CFST (Figure 52). It was displaced to a drift of 11.5% and a moment of 299 k-ft.

As for damage, this specimen began with a similar progression of damage as that observed for the first three specimens (initial vertical cracking and formation of 45-degree angle cracks); however, severe damage in the cap was not observed until after the formation of the plastic hinge within the CFST, and after reverse loading. The first cracks were observed in the cap at a moment of 92 k-ft (Figure 47), which was at the same load as that observed for the VT2/3-6 specimen. The propagation of the cracks through the cap and the formation of 45-degree angle cracks along the compression struts did not become extensive until a load of around 184 k-ft (Figure 48), significantly higher than that observed in the previous tests. A small gap began to form on the backside of the pile when the moment reached 230 k-ft but was not nearly as large as in the previous specimens. As stated above, besides this initial damage, little damage was observed in the cap until after the formation of the plastic hinges and reversed loading. The state of the cap at ultimate load can be observed in Figure 49 and Figure 50. Upon load reversal, the CFST again formed a plastic hinge (Figure 50); however, significantly more damage was observed in the cap (Figure 51, Figure 52, and Figure 53). The extensive damage observed in the cap indicates that the cap was near its capacity when a plastic hinge formed in the CFST.

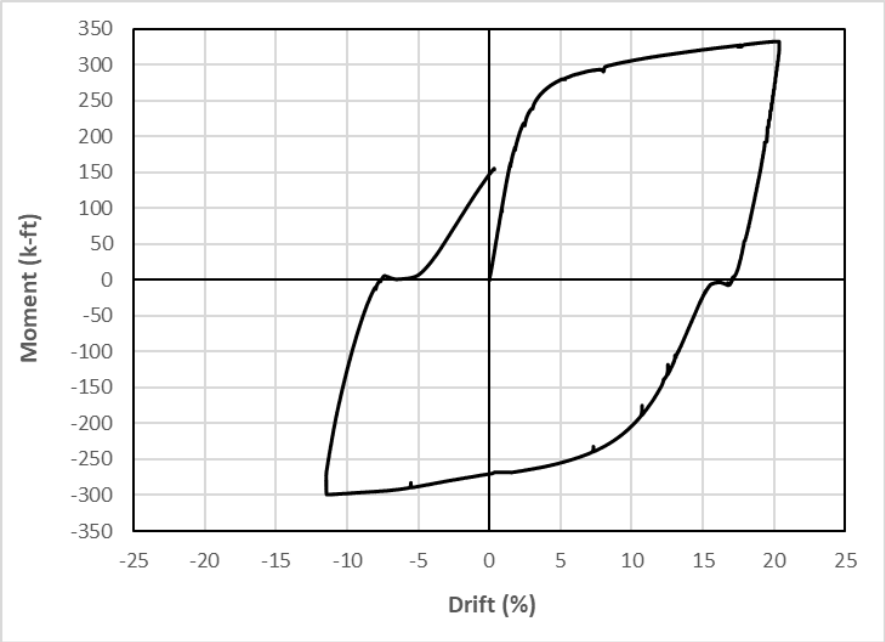


Figure 45: VT2/3-4U moment-drift curve

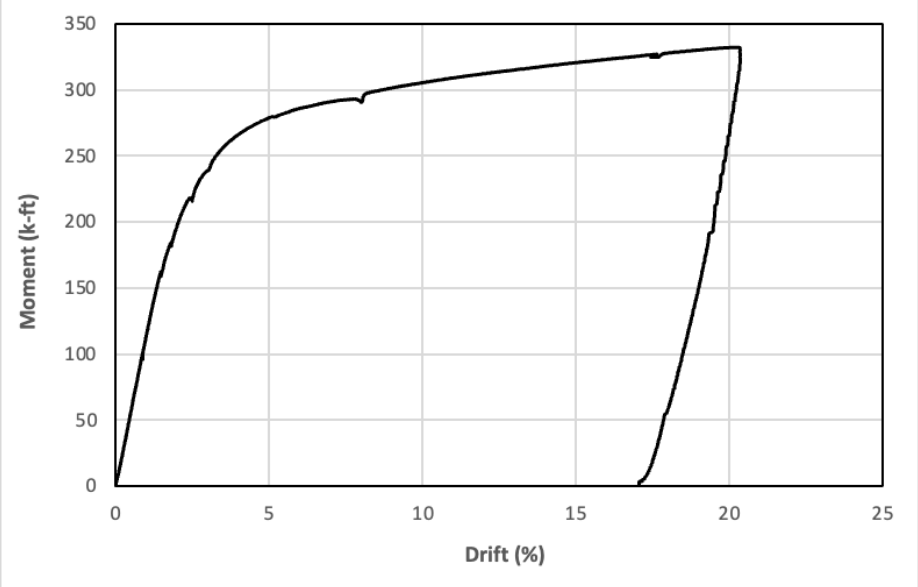


Figure 46: VT2/3-4U moment-drift curve (first pull)

Figure 47: VT2/3-4U first cracks (92 k-ft)

Figure 48: VT2/3-4U 45-degree cracks (184 k-ft)

Figure 49: VT2/3-4U buckling of CFST after formation of plastic hinge initial pull direction

Figure 50: VT2/3-4U failure from initial pull direction

Figure 51: VT2/3-4U buckling of CFST after formation of plastic hinge reverse push direction

Figure 52: VT2/3-4U failure from reverse push direction

Figure 53: VT2/3-4U prying action on back side of pile cap

# 5 DISCUSSION OF RESULTS

Key findings from this test series are discussed in this chapter. Specifically, the effects of varying scale, varying concrete strength, and including U-bars are evaluated. The efficacy of the newly developed methodology to predict cap capacity (moment-rotation) is then evaluated. For convenience, the overview of the test results is provided again in Table 2 along with predicted capacities (to be discussed in a following section).

Table 2: Summary of results including predicted capacities

| Specimen Name | Concrete Strength (psi) | Specimen Scale | Reinforcing Scheme | First Crack Moment (k-ft) | 45˚Crack Moment (k-ft) | Gap Formation Moment (k-ft) | Failure Mechanism | Ultimate Moment (k-ft) | Predicted Moment (k-ft) | Measured/Predicted Ratio |
|---|---|---|---|---|---|---|---|---|---|---|
| VT1/2-4 | 4000 | 1/2 Scale | Normal | 47.3 | 63 | 63 | Cap Failure/Crushing Cracking | 101.5 | 111.9 | 0.91 |
| VT2/3-4 | 4000 | 2/3 Scale | Normal | 69 | 115 | 92 | Cap Failure/Crushing Cracking | 208.3 | 232.5 | 0.90 |
| VT2/3-6 | 5500 | 2/3 Scale | Normal | 92 | 138 | 115 | Cap Failure/Crushing Cracking | 276.7 | 304 | 0.91 |
| VT2/3-4U | 4800 | 2/3 Scale | U-Bars Added | 92 | 184 | 230 | Plastic Hinge in CFT | 332.3 | 301.6 | 1.10 |
| | | | | | | | | | *Average =* | 0.95 |
| | | | | | | | | | *Coeff. Of Variation =* | 0.104 |

## 5.1 Effects of Specimen Scale

The test series began with a lightly reinforced half-size specimen (VT1/2-4) in part to ensure continuity between this test series (using a different loading setup) and those from previous MSU testing. It is difficult to directly compare measured responses from VT1/2-4 to previous testing due to numerous variations in testing parameters between the two series (e.g., embedment depths, reinforcing details, and axial load). However, the overall behavior and the observed progression of damage were similar, suggesting that the new loading setup effectively replicated the test conditions experienced by previous specimens.

The effect of scale can by isolated by comparing the first two specimens in this test series. That is, the only variation between the first specimen (1/2 size) and the second specimen (2/3$^{rd}$ size) was scale. For convenience, the measured moment-drift response for both tests are provided in Figure 54 and Figure 55. As expected, VT2/3-4 was significantly stiffer and stronger than the VT1/2-4. The ultimate moment capacity of VT2/3-4 was over twice that of VT1/2-4. While the differences in size make it difficult to directly compare the performance, both specimens demonstrated the same overall moment-drift response and progression of damage indicating that scale did not have a significant effect on the general behavior of the connection.

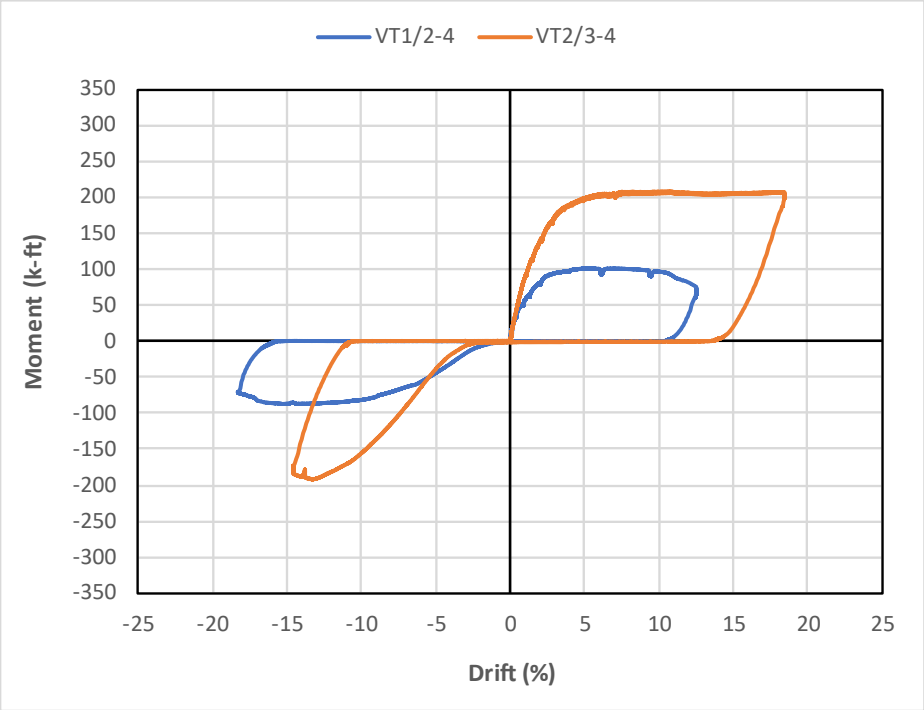


Figure 54: Moment-drift curve for VT1/2-4 and VT2/3-4

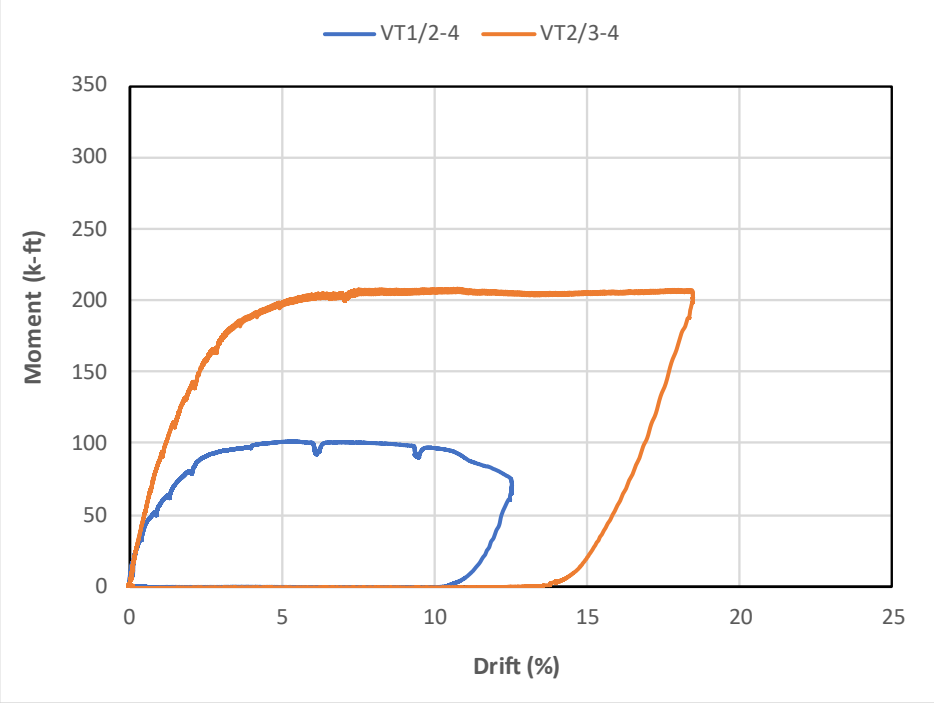


Figure 55: Moment-drift curve for VT1/2-4 and VT2/3-4 (first pull)

## 5.2 Effects of Concrete Strength

The effect of concrete strength was isolated with VT2/3-4 and VT2/3-6, where the only variation between these tests was concrete strength. VT2/3-4 had a concrete strength of 4 ksi, while VT2/3-6 had a target strength of 6 ksi (with an actual strength of 5.5 ksi). The moment-drift curves for these tests are provided in Figure 56 and Figure 57 for the overall response and the first pull, respectively. As can be observed in these figures and Table 2, both specimens demonstrated the same general behavior, had similar initial stiffnesses, and had similar failure mechanisms. That being said, VT2/3-6 had a significantly higher ultimate load than VT2/3-4, 276.7 k-ft versus 208.3 k-ft (an increase of approximately 33%). Similarly, damage initiated in VT2/3-6 at loads significantly higher than those observed for VT2/3-4, with initial cracks and the formation of 45-degree cracks occurring at loads 33% and 20% higher than VT2/3-4, respectively. It is worth noting that the concrete strength of VT2/3-6 (5.5 ksi) was 33% stronger than VT2/3-4 (4 ksi) on the day of testing, indicating that the effect that concrete strength has on cap performance may be approximately 1 to 1. That is, the concrete strength was 33% higher for VT2/3-6, as were the initiation of cracking and ultimate load, compared to VT2/3-4.

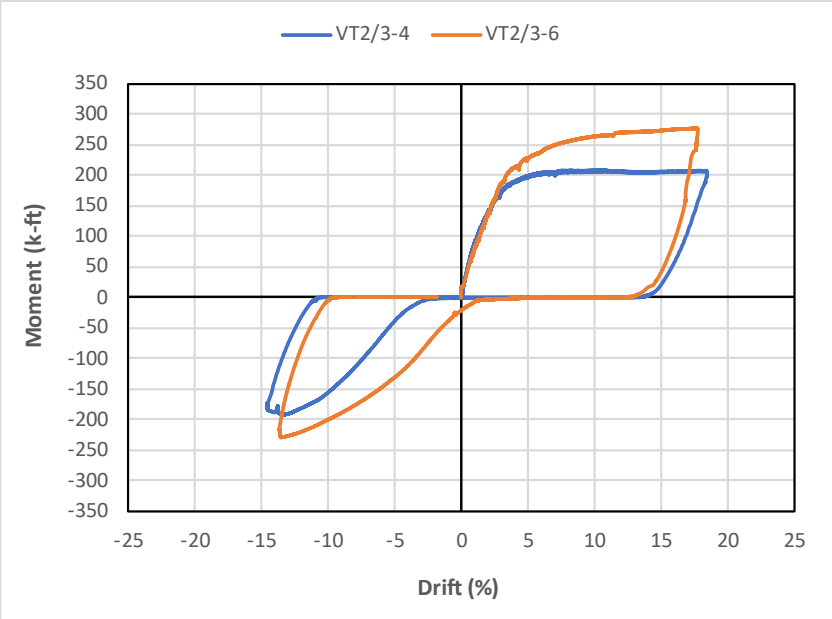


Figure 56: Moment-drift curve for VT2/3-4 and VT2/3-6

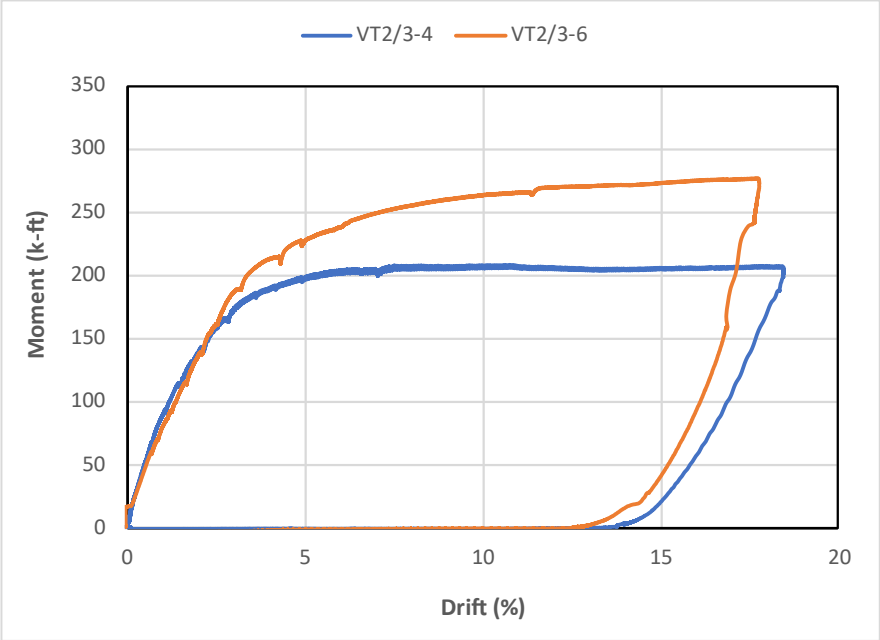


Figure 57: Moment-drift curve for VT2/3-4 and VT2/3-6 (first pull)

## 5.3 Effects of U-Bars

The effect of including U-bars within the cap can be isolated by comparing VT2/3-4 to VT2/3-4U. The moment-drift responses for these specimens are provided in Figure 58 and Figure 59. As can be observed in these figures and in Table 2, the general behavior of the specimens varied significantly. Specimen VT2/3-4U (including U-bars) was significantly stiffer and stronger than both VT2/3-4. The maximum moment observed for VT2/3-4U was 332.3 kip-ft versus the 208.3 k-ft observed for VT2/3-4 (an increase of around 60%). As stated previously, the concrete strength also varied for these specimens. The intended concrete strength for both specimens was 4 ksi; however, VT2/3-4U had a concrete strength of around 4.8 ksi on test day, a 20% difference. As was observed in the previous section, the effect of concrete strength was observed to be approximately linear; therefore, approximately 20% of the increased strength in this specimen may be attributed to this increased concrete strength. To further evaluate the effect of concrete strength, VT2/3-6 (5.5 ksi) is also included in these figures, as this specimen along with VT2/3-4 (4 ksi) brackets the concrete strength of VT2/3-4U (4.8 ksi). As can be observed, the increased concrete strength of VT2/3-6 results in an increased ultimate moment capacity, but it does not reach the same capacity observed for the U-bar specimen.

It should also be noted that the maximum moment observed in VT2/3-4U was obtained when the actuator reached its maximum stroke, prior to the specimen reaching its ultimate capacity. Additionally, the failure mechanism in this specimen was in the CFST and not in the cap; therefore, the actual cap capacity is unknown. That being said, the cap did fail upon the second pull cycle, indicating that the cap was near its capacity when the plastic hinge formed in the CFST.

Perhaps more notable than the differences in strength are the differences in observed failure mechanisms. The inclusion of U-bars in VT2/3-4U increased the cap capacity enough to force the failure into the CFST

(formation of a plastic hinge) rather than in the cap. Little damage was observed in the cap when the plastic hinge formed in this specimen. Because the CFST yielded prior to failure of the cap, the actual cap capacity is not known. That being said, significant damage was observed in the cap after the specimen was displaced to the extreme drift in the push direction and then returned to zero, again indicating that the cap was near its capacity when the plastic-hinge formed. It is also worth noting the differences in the cyclic response (hysteresis) of the two specimens. As would be expected for a specimen that formed a plastic hinge in a CFST, specimen VT2/3-4U had a robust hysteresis curve with no pinching, while VT2/3-4 had a significantly pinched response.

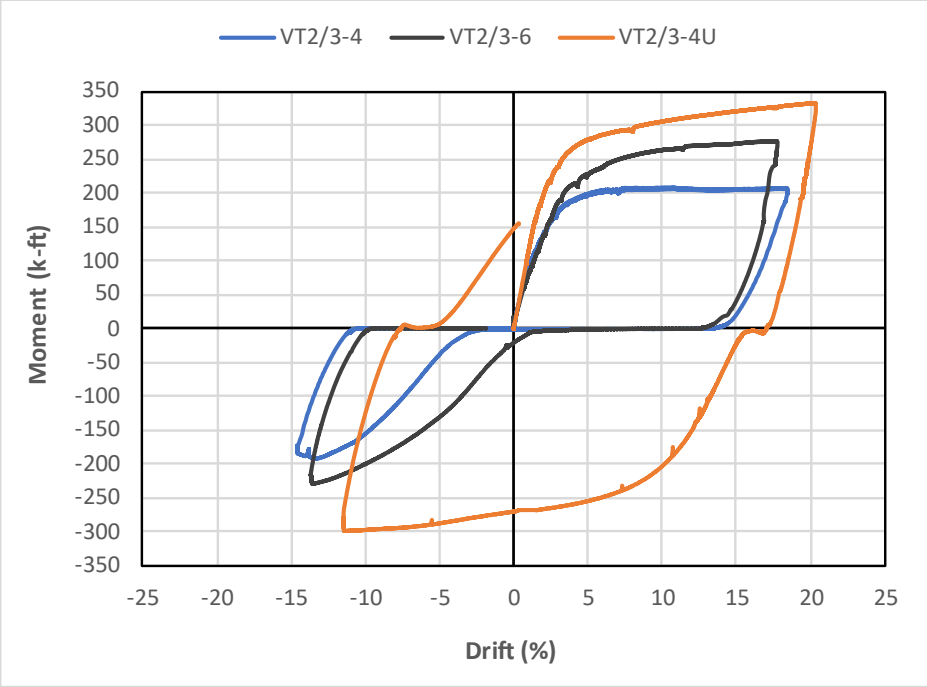


Figure 58: Moment-drift curve for VT2/3-4, VT2/3-6, and VT2/3-4U

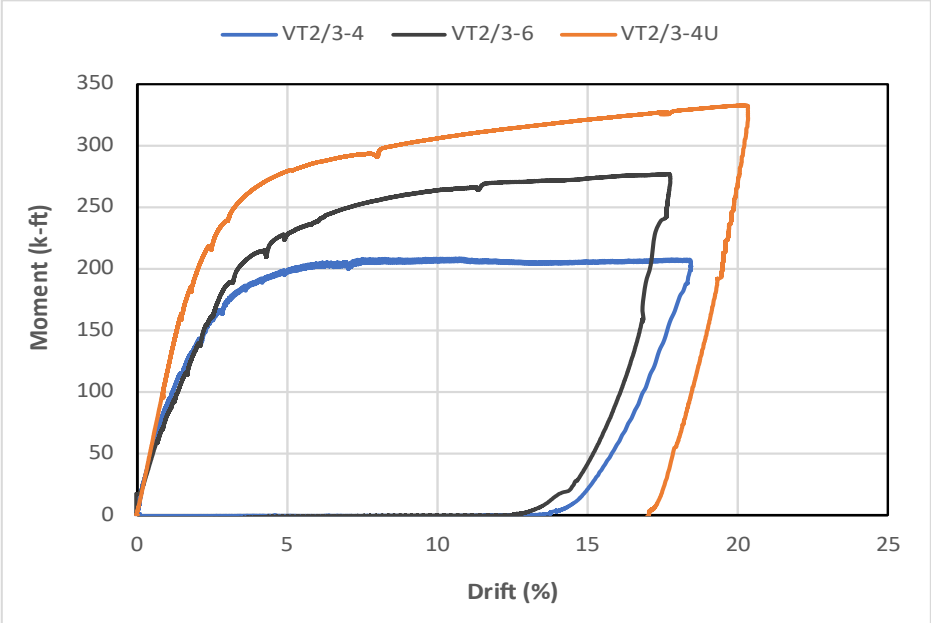


Figure 59: Moment-drift curve for VT2/3-4, VT2/3-6, and VT2/3-4U (first pull)

## 5.4 Efficacy of Moment-Rotation Methodology for Predicting Connection Capacity

### 5.4.1 Background

Previous research at MSU resulted in a simple moment-rotation methodology for predicting CFST to pile cap connection capacity [22]. This methodology takes an approach that closely resembles a moment-curvature analysis. Essentially, the moment and shear at the connection are resisted by the concrete immediately surrounding the embedded CFST and resisted by the U-bars (if included), as shown in Figure 60. To start, the connection elements within the cap are discretized into individual fibers with corresponding stress-strain responses. A fixed rotation is then applied to the embedded CFST. Subsequently, the strains in the cap's individual fibers are determined through this rotation (as shown in Figure 61) and applying strain-displacement compatibility. The resulting stresses from these strains are then calculated using their corresponding nonlinear material responses. Resultant forces are calculated by multiplying these stresses by the corresponding fiber areas. This method ensures equilibrium between the resultant forces and the external shear and moment applied by the CFST, employing a double-iterative process that adjusts both the rotation angle and the rotation location until equilibrium is achieved. The resultant forces acting on the embedded CFST for each fiber are shown in Figure 62.

This method was initially evaluated/calibrated by comparing the measured and predicted ultimate capacities from a data set of 9 previous CFST pile cap connection tests conducted at MSU. It was found that the proposed methodology closely predicted the actual capacity across the wide range of reinforcing schemes (with- out U-bars, with U-bars, and with a double set of U-bars), concrete strengths, and embedment depths considered in the tests, with an average measured to the predicted ratio of 0.99 with a coefficient of variation of 5.4%. While this finding was promising, it was determined that this methodology should be evaluated over a wider range of variables and a different test setup; hence the research conducted herein.

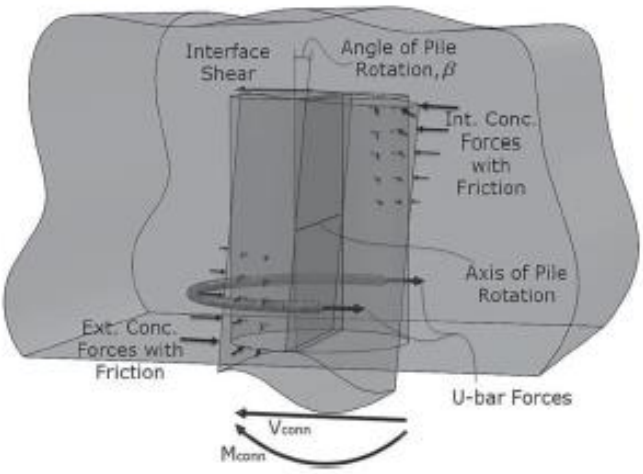


Figure 60: Imposed rotation and resultant internal forces and stresses [22]

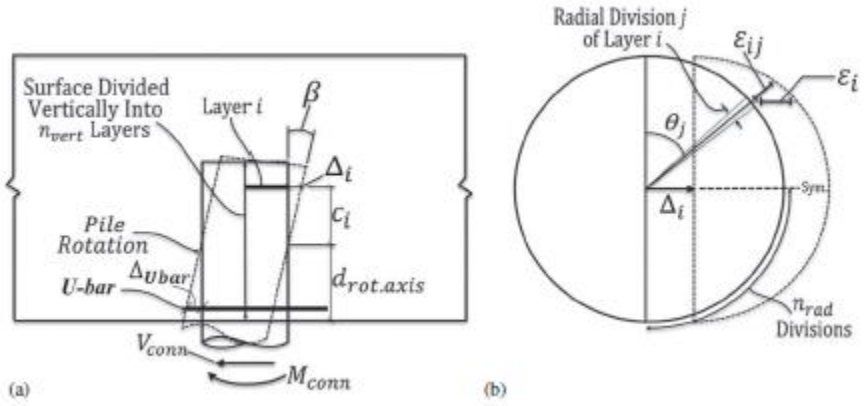


Figure 61: Pile rotation, displacements, and radial strain distribution: (a) front view of the embedded pile; and (b) top view of i$^{th}$ pile surface layer [22]

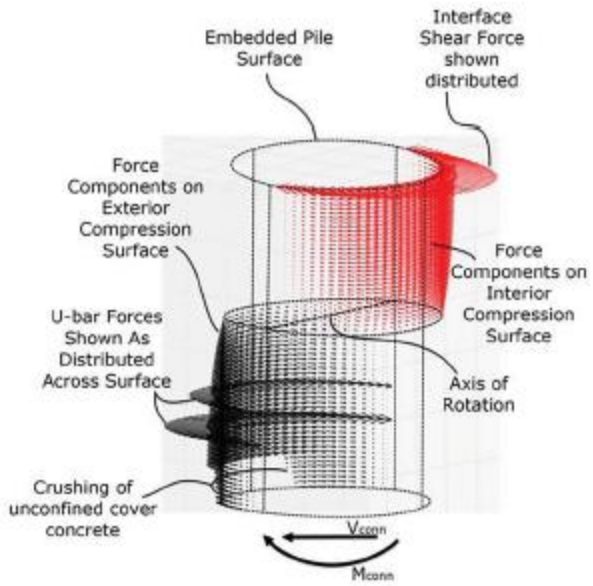


Figure 62: Internal forces acting on the embedded end of the pile [22]

### 5.4.2 Evaluation of Measured versus Predicted Capacity

The moment-rotation methodology was applied to the specimens in this test series and compared to their measured capacities to further evaluate the efficacy of this method for predicting the capacity of CFST to cap connections. Input and output from the program used to implement this methodology is provide in Appendix A. Table 2 provides the measured and predicted ultimate capacities for these specimens, along with the ratios of measured to predicted. As can be observed in this table, the average measured-to-predicted ratio for all specimens was 0.95 with a coefficient of variation of 10%, indicating that this methodology is effective at predicting the capacity of the specimens in this test series. That being said, it's worth noting that for the specimens not including U-bars, this methodology overpredicted the capacities of the connections, with an average measured-to-predicted ratio of 0.9. That is, these specimens failed prior to reaching their predicted capacities. This phenomenon may possibly be attributed to mechanisms not currently accounted for in the current analysis methodology. That is, the current methodology, as imposed here, does not take into consideration the global flexural failure of the cap, and the role that the longitudinal reinforcement plays in preventing this mechanism. It should be noted that this failure mechanism was observed in the first three specimens tested in this series, indicated by the flexural cracks forming over the height of the specimen at failure.

Further, this methodology underpredicted the capacity of the specimen that included U-bars (VT2/3-4U) by around 10%. This assumes that VT2/3-4U was near the cap capacity when the specimen reached its maximum observed moment. This should be investigated further to determine any possible causes for this phenomenon. It is also worth noting that besides the inclusion of U-bars, the parameters varied in this research (i.e., scale, load setup, and concrete strength) did not appear to directly affect the accuracy of this methodology.

### 5.4.3 Brief Parametric Study Evaluating the Sensitivity of Moment-Rotation Methodology

A further assessment of the moment-rotation methodology was conducted to provide insight into which variables have the largest impact on the predicted capacity of the system. The variables evaluated in this parametric study were embedment depth of the pile into the cap, concrete strength, and U-bar size/area. In this study, each variable was systematically adjusted, and the resultant ultimate capacity calculated with the moment-rotation methodology was recorded. This predicted ultimate capacity was then compared to the predicted ultimate capacity of a standard/datum cap. This standard cap had the same general properties as our 2/3$^{rd}$ scale specimens, which had an embedment depth of 50% of the depth of the cap, a concrete strength of 4 ksi, and no U-bars. The effect of each parameter was evaluated by plotting the ratio of the predicted ultimate moment to the predicted moment of the datum specimen versus the variable being evaluated. The effect of each parameter is discussed in detail below.

#### 5.4.3.1 Embedment Depth

Embedment depth was defined in terms of percentage of the depth of the concrete cap. This parameter was evaluated by varying embedment depth while keeping all other variables held constant. This parameter varied between 25% to 75% of total cap depth. The ratios of capacity to standard cap capacity are plotted below versus the embedment depth (Figure 63). Referring to this figure, as expected, an increase in embedment depth results in a significant increase in predicted capacity. Specifically, decreasing the embedment depth to 25% of the pile cap depth (a 50% decrease relative to standard specimen) resulted in a moment ratio of 0.23. Conversely, increasing the embedment depth to 75% of cap depth (a 50% increase relative to standard specimen) resulted in moment ratio of 2.26.

#### 5.4.3.2 Concrete Strength

The effect of concrete strength on the predicted capacity was evaluated by varying concrete strength from 3 ksi to 10 ksi, while holding all other parameters constant. The ratios of predicted moment to predicted moment of the standard specimen are plotted versus concrete strength in Figure 64. As can be observed and as expected, the predicted moment increased with concrete compressive strength. The moment ratio was observed to increase from 0.84 at a concrete strength of 3 ksi (75% of the standard specimen) to a ratio of 1.78 at a concrete strength of 10 ksi (an increase in strength of 150% relative to standard specimen).

Note that this relationship is not 1 to 1, as observed during testing. That is, a percent increase in concrete strength does not result in an equal percent increase in capacity. The measured test results indicated that a 33% increase in concrete strength resulted in a 33% increase in ultimate capacity. According to this parametric study the same increase in concrete strength would result in an increased capacity of 22%.

#### 5.4.3.3 U-Bar Size

The effect that the amount of U-bar reinforcement has on predicted capacity was evaluated by varying the area of U-bar reinforcement while holding all other parameters constant. Figure 65 is a plot of the moment ratio versus the x-sectional area of on leg of U-bar reinforcement. Note that the standard specimen did not include U-bar reinforcement, and therefore has a U-bar area of 0. Also note that the U-bar configuration used in this calculation was the same as that used in VT2/3-4U, which included four total U-bars, a pair bars near the tip of the embedded pile and a pair near the surface of the pile. As can be observed in this

figure, the moment was observed to increase linearly with increasing U-bar area. The moment ratio increased from 1.0 for the standard specimen to 1.5 for U-bar area of 1.27 $in^2$ (#10 rebar). It should be noted that including #6s (as was done for VT2/3-4U resulted in a moment ratio of 1.18. However, the increase in capacity observed in the measured test results (by comparing VT2/3-4 with VT2/3-4U) was significantly higher than this, with an observed increase of 50% when U-bars were included. This assumes that VT2/3-4U was near the cap capacity when the specimen reached its maximum observed moment.


Figure 63: Effects of embedment depth on ultimate capacity

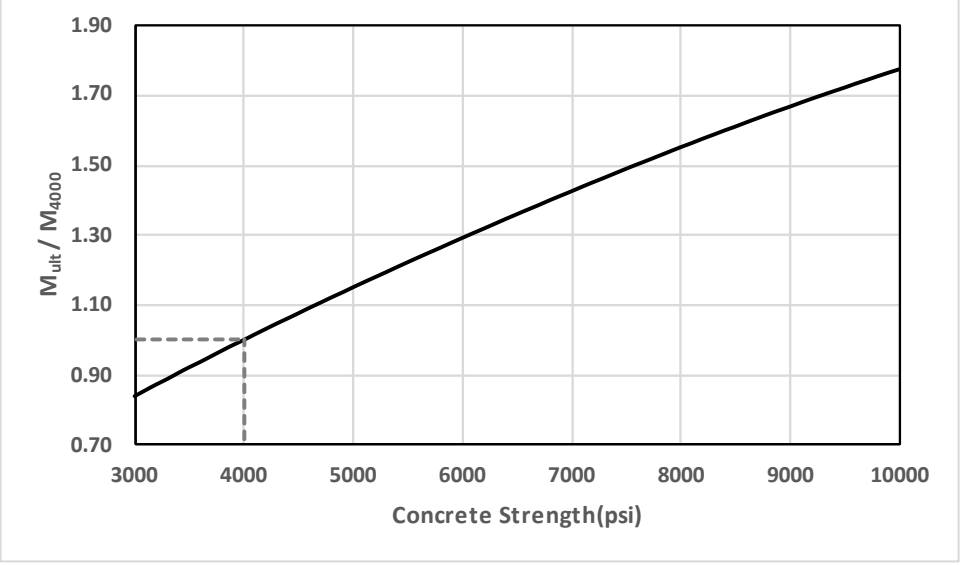


Figure 64: Effects of concrete strength on predicted ultimate capacity


Figure 65: Effects of U-bar size on predicted ultimate capacity

#### 5.4.3.4 Summary of Parametric Study

This parametric study quantified the effects that embedment depth, concrete strength, and amount of U-bar reinforcement have on predicted capacities of the CFST to pile cap connections. While all studied parameters influenced the predicted capacity (as expected), the embedment depth was shown to have the largest effect, with an increase in strength of 126% for an increase of embedment depth of only 50%. Whereas an increase in concrete strength of 150% only resulted in an increase in cap capacity of 78%. The increase in capacity resulting from the inclusion of U-bars was significant but was not as significant as what was observed in the test specimens. Specifically, the inclusion of #6 U-bars in the test specimens (VT2/3-4 vs VT2/3-4U) resulted in an increase in capacity of 50% (although some of this may be attributed to the increased concrete strength in this specimen which was around 20%). However, including #6 U-bars only increased the predicted capacity by 18%.

# 6 SUMMARY AND CONCLUSIONS

This project began with a brief literature review focused on previous pile cap research that has been conducted since the completion of the previous phases of this research. Subsequently, four pile cap connection specimens were designed and tested to evaluate the effects that several model parameters (i.e., scale, concrete strength, inclusion of U-bars) may have on connection performance. These tests were then used to evaluate the efficacy of a newly developed moment-rotation methodology for predicting cap capacity. Based on this research, the following conclusions can be made:

1) Apart from the specimen including U-bars, all specimens demonstrated the same overall moment-drift response, progression of damage, and failure mechanism. In these specimens, damage initiated with the formation of cracks on the side of the cap, which progressed into the expansion of these cracks and the formation of 45-degree angle cracks propagating along compression struts on the bearing side of the pile. Failure in the specimens ultimately occurred due to a combination of (1) concrete crushing on the bearing side of the pile and on the backside of the pile near the tip of the embedded pile, (2) tension cracks on the backside of the pile that extended the full height of the specimen, and (3) 45-degree angle cracks propagating along compression struts originating from the pile to the edge of the cap.

2) The inclusion of U-bars increased the capacity of the cap enough to force the failure mechanism of the specimen into the CFST pile, which failed due to the formation of a plastic-hinge. The inclusion of U-bars increased the cap capacity by around 50%.

3) Specimen scale was observed to have a significant effect on connection performance (as expected), with the larger specimens having higher stiffness and strength relative to the smaller size specimen. That being said, both scales exhibited similar overall moment-drift responses and patterns of damage progression, indicating that besides the obvious increased strength and stiffness, scale did not affect the performance of the connection.

4) An increase in concrete strength from 4 ksi to 5.5 ksi (a 33% increase) led to approximately a 33% increase in the initiation of damage and ultimate load capacity. This indicates that the effect of concrete strength on cap performance may be 1 to 1. However, the parametric study on the analytical moment-rotation methodology indicated otherwise.

5) A notable influence of U-bars was observed in the tests. Their inclusion significantly enhanced the stiffness and strength of the specimens, evidenced by the increased cap capacity, and altered failure mechanisms. In addition to providing confinement in the connection zone, the U-bars may also be providing reinforcement to resist global bending moments observed in the cap. The shift in failure point from the cap to the formation of a plastic hinge in the CFST also positively affected the hysteresis behavior.

6) Regarding the moment-rotation methodology, the study found it to be highly accurate in predicting the capacities of cap connections, with an average measured-to-predicted ratio of 0.95. However, the methodology tends to overpredict capacities for connections without U-bars and underpredict for those with U-bars, indicating a need for further refinement. The overprediction of capacities may be attributed to the fact that global flexural failures are not accounted for in the current

methodology, as implemented, and does not consider the role that the longitudinal reinforcement plays in preventing this mechanism. Additionally, no obvious trend was observed in this methodology's accuracy with varying scale or concrete strength.

7) The parametric study investigated the effects of various parameters on the predicted capacities of the connections; specifically, it quantified the effects that embedment depth, concrete strength, and amount of U-bar reinforcement have on predicted performance. This study demonstrated that while all studied parameters influenced the predicted capacity, embedment depth had the most effect on capacity, with an increase in strength of 126% and corresponding increase of embedment depth of 50%.

Overall, this research provides substantial insights into the behavior of CFST to concrete pile cap connections under various conditions and validates the use of the moment-rotation methodology as a reliable tool for capacity prediction. Future research should focus on investigating the discrepancies in predictions, particularly concerning the inclusion of U-bars and the possible modifications to this methodology to account for this phenomenon.

# 7 REFERENCES


1. Kappes, L., M. Berry, and J. Stephens, *Performance of Steel Pipe Pile-to-Concrete Cap Connections Subject to Seismic or High Transverse Loading: Phase III Confirmation of Connection Performance*. 2013, Montana Department of Transportation.

2. Li, X., et al., *Structural behavior of double-CFST-pile foundations under cyclic loads.* Soil Dynamics and Earthquake Engineering, 2020. **128**.

3. Xian, L., et al., *Punching shear strength of CFST bridge column to reinforced concrete four-pile cap connections.* Journal of Bridge Engineering, 2017. **22**(8): p. 04017036 (11 pp.).

4. Kingsley, A., *Experimental and Analytical Investigation of Embedded Column Base Connections for Concrete Filled High Strength Steel Tubes*, in *Civil and Environmental Engineering*. 2005, University of Washington.

5. Williams, T., *Experimental Investigation of High Strength Concrete Filled Steel Tubes in Embedded Column Base Foundation Connections*, in *Civil and Environmental Engineering*. 2007, University of Washington.

6. Lee, J., *Experimental investigation of embedded connections for concrete filled tube column connections to combined axial–flexural loading*. 2011, University of Washington.

7. Lehman, D.E. and C.W. Roeder, *Foundation connections for circular concrete-filled tubes.* Journal of Constructional Steel Research, 2012. **78**: p. 212-225.

8. McFarlane, I.S., *Non-Linear Finite Element Analysis of Concrete Filled High Strength Steel Tubes: Structural Performance and Sensitivity to Design Parameters*. 2006, University of Washington.

9. Roeder, C.W., D.E. Lehman, and R. Thody, *Composite Action in CFST Components and Connections.* Engineering Journal-American Institute of Steel Construction Inc, 2009. **46**(4): p. 229-242.

10. Moon, J., et al., *Strength of Circular Concrete-Filled Tubes with and without Internal Reinforcement under Combined Loading.* Journal of Structural Engineering, 2013. **139**(12).

11. Roeder, C.W., M.T. Stephens, and D.E. Lehman, *Concrete filled steel tubes for bridge pier and foundation construction.* International Journal of Steel Structures, 2018. **18**(1): p. 39-49.

12. Stephens, M.T., *Design Expressions and Dynamic Evaluation of CFST Bridges Subjected to Seismic Hazards*. 2016, University of Washington.

13. Stephens, M.T., et al. *Seismic Design of Circular Concrete Filled Tube Bride Pier Connections for Accelerated Bridge Construction*. 2014. Reston, VA, USA: American Society of Civil Engineers.

14. Stephens, M.T., et al., *Seismic CFST Column-to-Precast Cap Beam Connections for Accelerated Bridge Construction.* Journal of Structural Engineering, 2016. **142**(9).

15. Stephens, M.T., D.E. Lehman, and C.W. Roeder, *Design of CFST column-to-foundation/cap beam connections for moderate and high seismic regions.* Engineering Structures, 2016. **122**: p. 323-337.

16. Stephens, M.T., D.E. Lehman, and C.W. Roeder, *Seismic performance modeling of concrete-filled steel tube bridges: Tools and case study.* Engineering Structures, 2018. **165**: p. 88-105.

17. Zhu, H., et al., *Inelastic response prediction of CFST columns and connections subjected to lateral loading.* Journal of Constructional Steel Research, 2017. **132**: p. 130-140.

18. WASHDOT, *Bridge Design Manual*. 2019, Washington State Department of Transportation.

19. Kappes, L., et al., *Seismic performance of concrete-filled steel tube to concrete pile-cap connections.* Journal of Bridge Engineering, 2016. **21**(7): p. 04016042 (17 pp.).

20. Kappes, L., et al., *Concrete Filled Steel Tube Piles to Concrete Pile-Cap Connections*, in *ASCE/SEI Structures Congress*. 2012: Chicago, Ill.

21. Stephens, J. and L. McKittrick, *Final Report: Performance Of Steel Pipe Pile-To-Concrete Bent Cap Connections Subject To Seismic Or High Transverse Loading*. 2005, Montana Department of Transportation.

22. Kappes, L., et al., *Simple Moment-Rotation Methodology for Predicting the Capacity of Concrete-Filled Steel Pipe Piles to Concrete Cap Connections.* Journal of Bridge Engineering, 2021. **26**(10).

# APPENDIX A: PREDICTED CAPACITY ANALYSIS VIA MOMENT-ROTATION METHODOLOGY

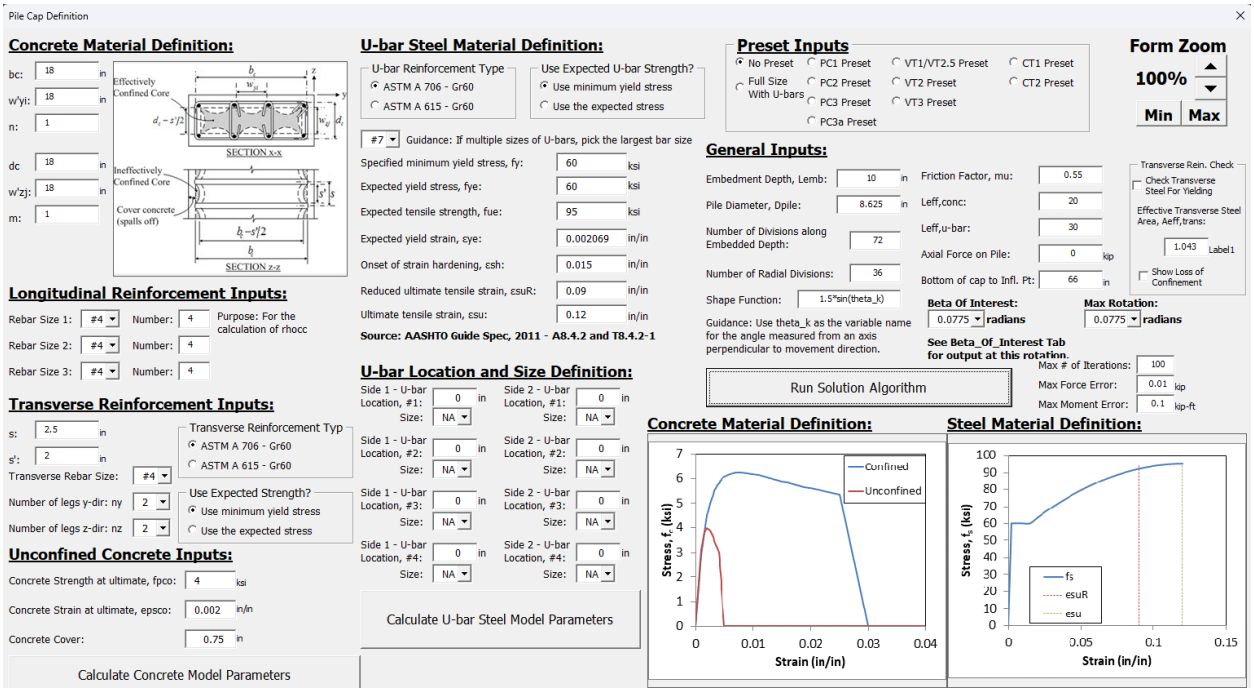


Figure 66: Input for VT1/2-4

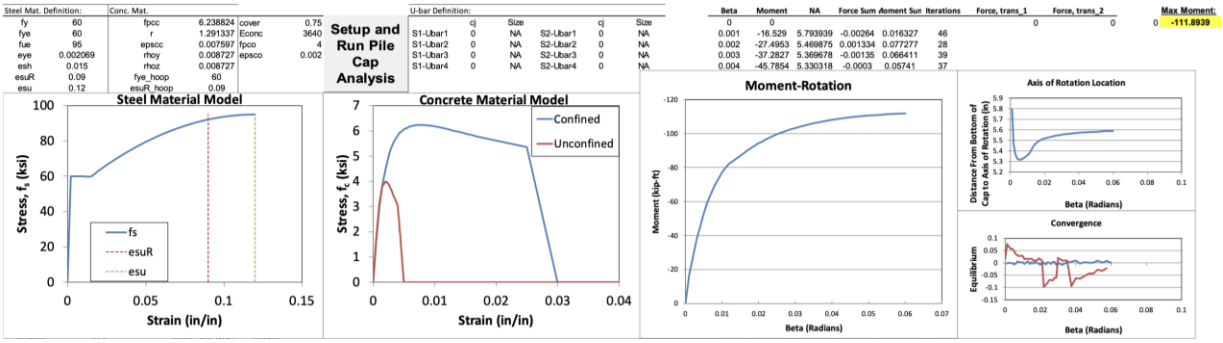


Figure 67: Output for VT1/2-4

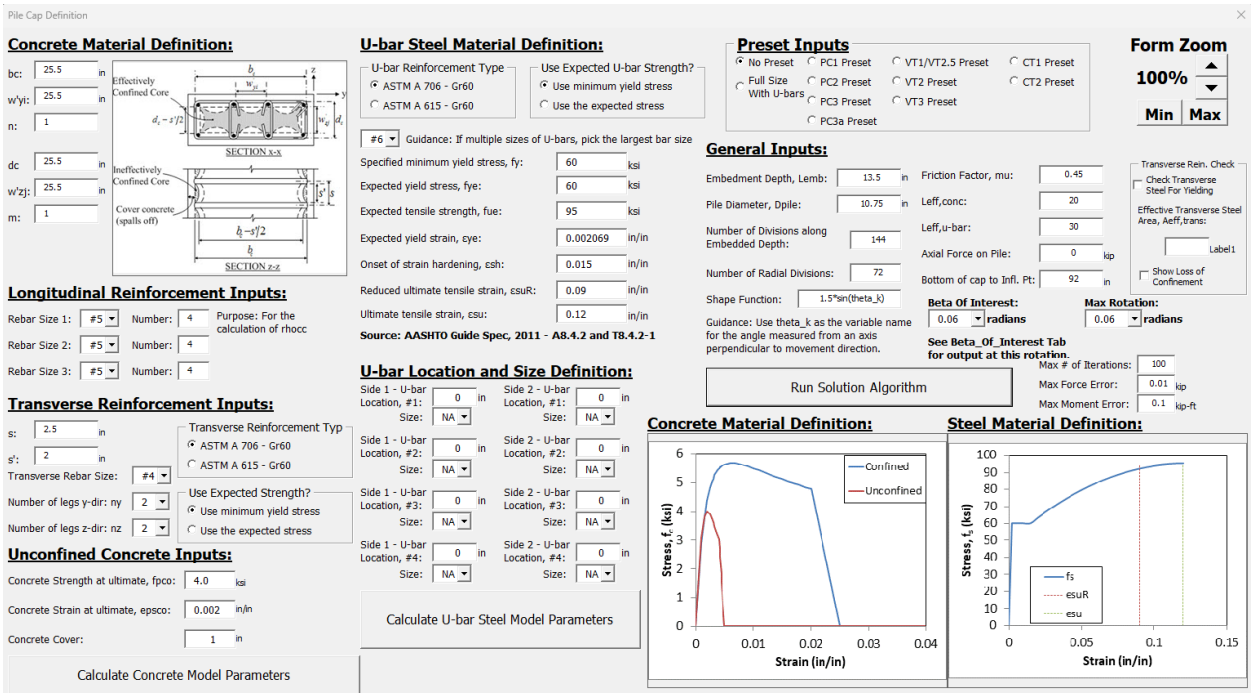


Figure 68: Input for VT2/3-4

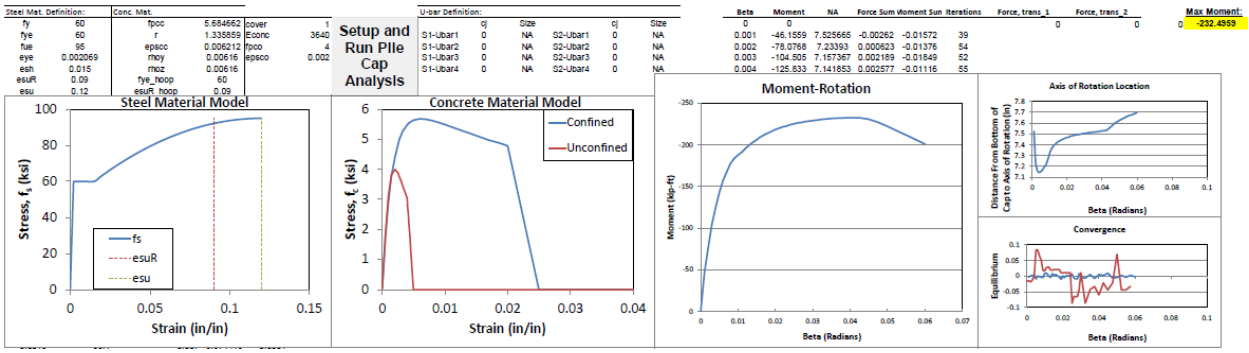


Figure 69: Output for VT2/3-4

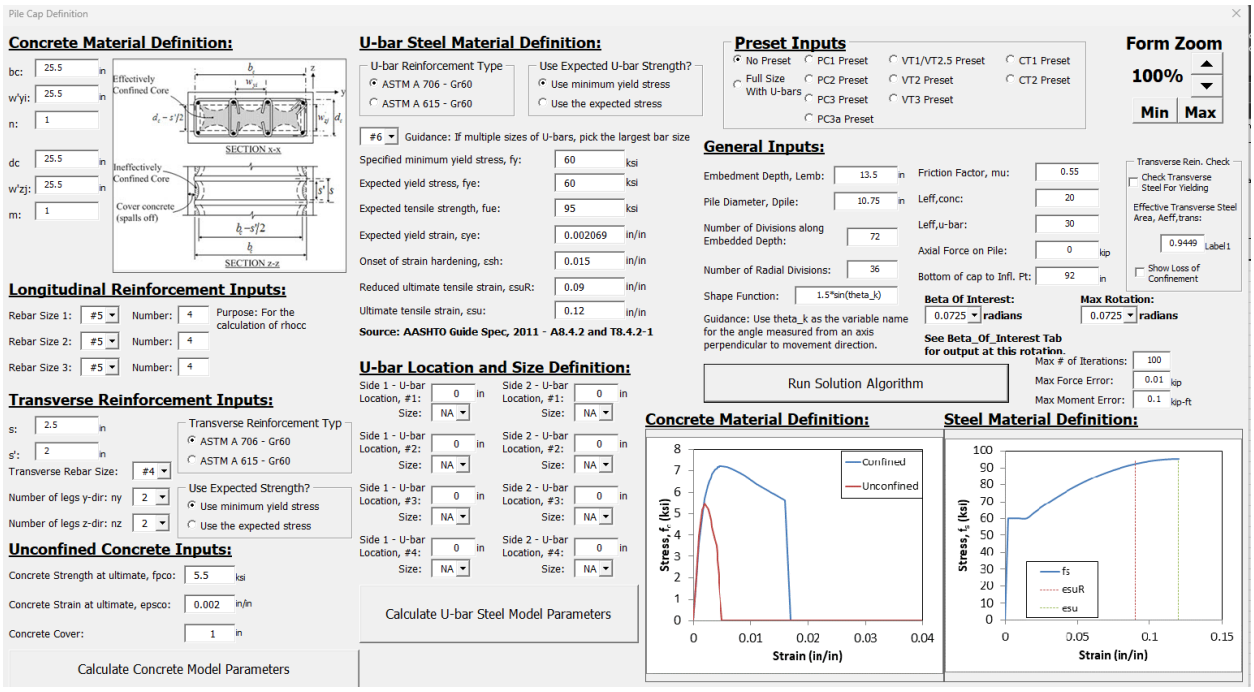


Figure 70: Input for VT2/3-6

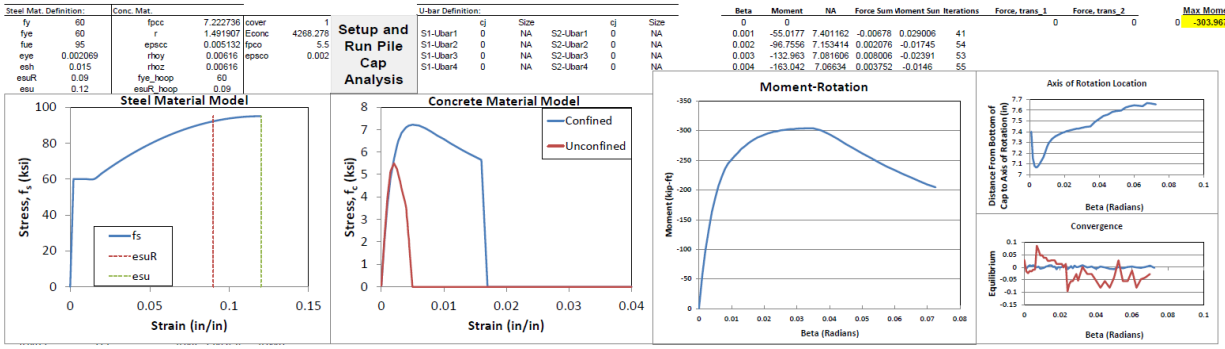


Figure 71: Output for VT2/3-6

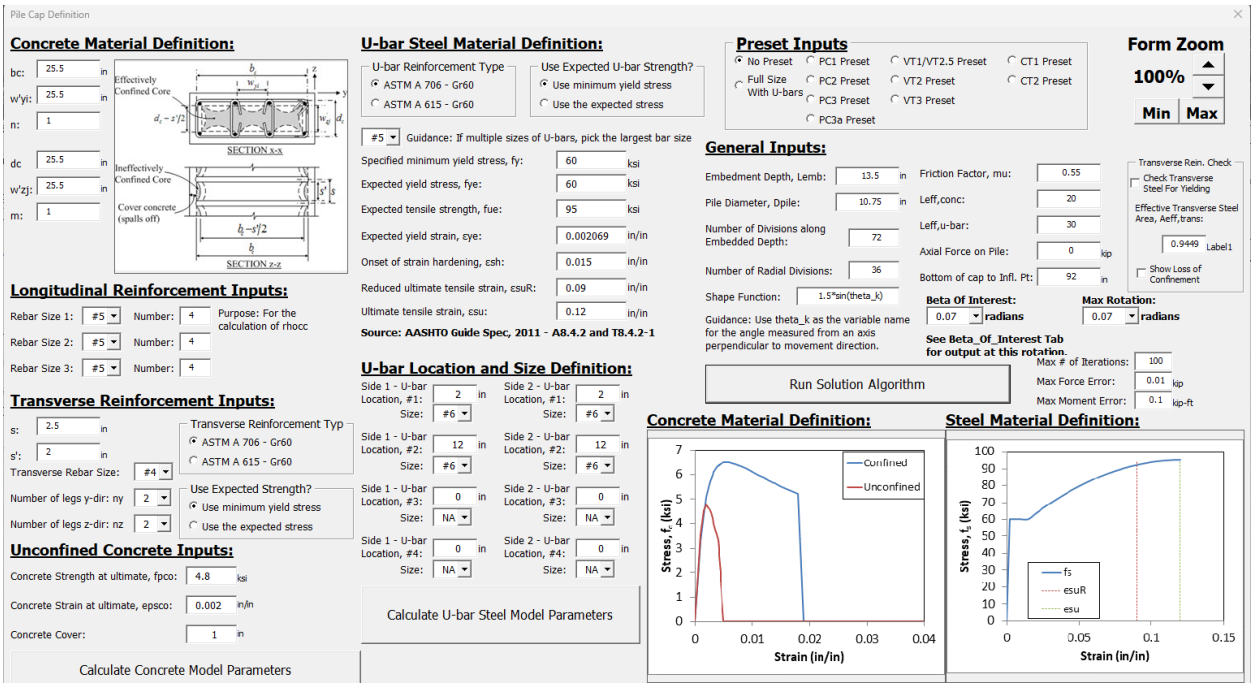


Figure 72: Input for VT2/3-4U

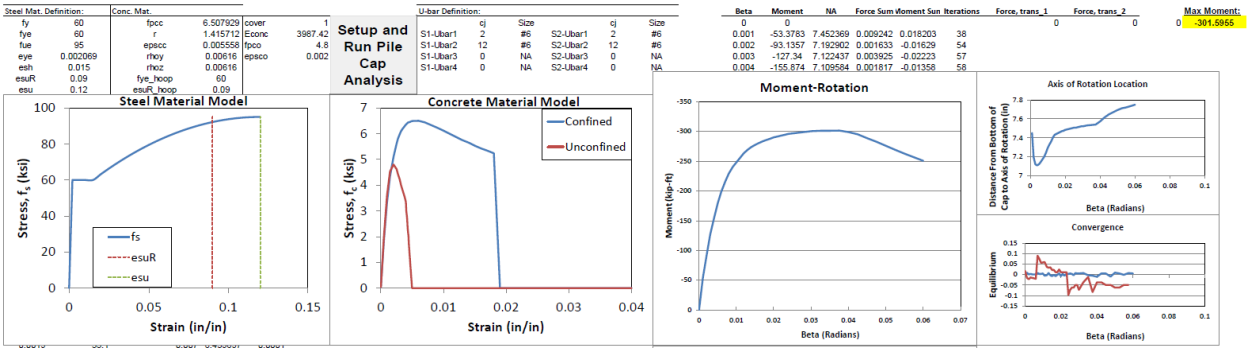


Figure 73: Output for VT2/3-4U